Master's Thesis
Master's Programme in Atmospheric Sciences
Meteorology

Arctic Air Mass Characteristics Based on Observations at SMEAR I in 1998-2017

Pyry Poutanen

May 11, 2019

Supervisors: Prof. Tuukka Petäjä
Doc. Victoria Sinclair

Examiners: Prof. Veli-Matti Kerminen
Doc. Jouni Räisänen

University of Helsinki
Faculty of Science

PL 64 (Gustaf Hällströmin katu 2a)
00014 Helsingin yliopisto

HELSINGIN YLIOPISTO — HELSINGFORS UNIVERSITET — UNIVERSITY OF HELSINKI

Tiedekunta — Fakultet — Faculty	Koulutusohjelma — Utbildningsprogram — Degree programme
Faculty of Science	Master's Programme in Atmospheric Sciences Meteorology

Tekijä — Författare — Author

Pyry Poutanen

Työn nimi — Arbetets titel — Title

Arctic Air Mass Characteristics Based on Observations at SMEAR I in 1998-2017

Työn laji — Arbetets art — Level	Aika — Datum — Month and year	Sivumäärä — Sidantal — Number of pages
Master's Thesis	May 11, 2019	56

Tiivistelmä — Referat — Abstract

The Arctic is warming faster than any other region on Earth due to climate change. The characteristics of the air masses overlying the Arctic play a key role when assessing the magnitude and implications of global warming in the region, but comprehensive studies of Arctic air mass properties covering long time series of measurements are scarce. The aim of this study is to use such a data set to quantify the key characteristics of Arctic air masses prior to transport to the human-habited Eurasian continent, and the typical conditions leading to Arctic events in Värriö.

HYSPLIT (Hybrid Single Particle Lagrangian Integrated Trajectory) model was employed to calculate backward atmospheric trajectories arriving at SMEAR I (Station for Measuring Ecosystem-Atmosphere Relations) in Värriö for every hour in 1998-2017. An air mass was classified as Arctic if the backward trajectory arriving at Värriö was located north of 78 °N 72 hours before the arrival time. Data from SMEAR I, including meteorological variables and trace gas and aerosol concentrations, were then gathered in order to compare Arctic and non-Arctic air masses.

Of all the hours that were analysed, 15.0 % were classified as associated with an Arctic air mass. The typically cyclonic curvature of the trajectories and the median duration of 10 hours per individual Arctic event were hypothesised to be due to Arctic air mass events being linked to passing low pressure systems. Arctic air masses were found to be colder and have lower moisture content in summer, when the difference at surface level was 5.6 °C and 1.7 g m^{-3} respectively, compared to non-Arctic air masses. In other seasons the differences were less pronounced, but average particle and trace gas concentrations were found to be notably lower for Arctic air masses than for non-Arctic air masses. An exception to this was ozone, which had 24.6 % higher average concentration in Arctic air masses in months between November and February, compared to non-Arctic air masses. The annual median aerosol particle concentration in Arctic air masses was found to be 308 cm^{-3} and only 129 cm^{-3} between November and March, on average. During a median year, the value of condensation sink (CS) was on average 65 % smaller in Arctic air masses than in the non-Arctic. The Kola Peninsula industry was observed to increase concentrations of SO_2 and aerosol particles, particularly Aitken mode (25-90 nm) particles, of affected air masses.

Overall, Arctic air masses were found to have several unique characteristics compared to other air masses arriving at SMEAR I, Värriö. As expected, Arctic air masses are colder and drier than non-Arctic air masses, but the difference is pronounced only in summer months. Other air mass characteristics, especially aerosol particle and trace gas concentration were generally found to be lower, unless the air mass was influenced by the industrial sites in the Kola Peninsula.

Avainsanat — Nyckelord — Keywords

Arctic, aerosol measurements, air mass, back trajectories, SMEAR

Säilytyspaikka — Förvaringsställe — Where deposited

Muita tietoja — Övriga uppgifter — Additional information

Contents

1. Introduction

The Arctic is extremely vulnerable to global warming and rapid changes have already been observed there (ACIA, 2004). One of the largest sources of uncertainty in climate change is the effect of aerosol particles on the radiative balance (Lohmann and Feichter, 2005). The aerosol loading by humans in the Arctic is low due to almost non-existent human settlements in the region, but sources of natural aerosols exist and they are a matter of uncertainty, too (Carslaw et al., 2013). In the warming Arctic climate, an increasing fraction of the sea will remain open, which would further enhance natural aerosol sources (Mauritsen et al., 2011). To fully assess the current and future state of the Arctic, meteorological observations alone are not enough, they need to be combined with observations of aerosols and trace gases.

Only few long-term measurement stations are located in the high latitudes to allow observations of Arctic air masses before they are notably modified by the mid-latitude biosphere and human activities. Station Nord in Greenland (81°36'N, 16°40'W), Zeppelin station in Svalbard (78°58'N, 11°53'E) and Alert station in Canada (82°27'N, 62°32'W) are examples of such stations. These Arctic stations are often used for measurement campaigns (e.g. King and Simpson, 2001), but the variety of long-term measurements remains narrow.

Over 20 years of measurements have been conducted at a measurement station, SMEAR I (67°46'N, 29°36'E), in Eastern Lapland (Hari et al., 1994). A comprehensive set of variables have been measured all-year round to understand relationships between the biosphere and the atmosphere. The station is located in the border region of maritime Arctic air masses and the human habited continent, which makes the measurements suitable for studying Arctic air masses.

Air mass classification is traditionally done using only temperature and humidity (Bergeron, 1930) and by that classification, Arctic air masses are classified as colder than other air masses. However, sometimes no separation is made between Arctic and continental polar air masses, as they can both be very cold in winter (Curry, 1983). The traditional classification method can be especially problematic in Finland, as both air masses are frequently observed and the open Arctic Ocean introduces fluxes of heat and moisture from the sea surface to arriving air masses, which makes the temperature-based distinction more difficult.

To avoid the use of temperature in the identification of Arctic air masses, a trajectory-based method was used. Tracking the path of an air particle backwards in time allows us to obtain an estimate of its region of origin. If the Arctic is defined to be located above a threshold latitude, identification can be done. The measurements at SMEAR I can then be used to study Arctic air mass characteristics at the gateway to the Eurasian continent, as it is possible to determine the exact times when conditions are associated with Arctic air masses.

The main aim of this thesis is to study what unique characteristics Arctic air masses have compared to non-Arctic air masses in a high-latitude boreal forest environment, based on observations at SMEAR I. In addition to temperature and humidity, which are traditionally used as the basis for air mass classification, other possible properties to use for Arctic air mass identification are assessed. Especially the concentrations of aerosol particles and trace gases are analysed and also the relevance of trajectory path regarding major anthropogenic pollution sources in the Kola Peninsula is examined. Another aim of the study is to find typical trajectory paths and conditions leading to Arctic air mass events, and how anthropogenic pollution sources in the Kola Peninsula can affect air mass properties along the trajectory.

In chapter 2 some essential background to air masses in general and the used methods are introduced. The station environment and measurements are described in detail in chapter 3. Following that, the data processing steps taken to separate Arctic air masses from other air masses are explained. In chapter 4, the results are shown starting from trajectory statistics and then moving on to the different characteristic meteorological and air composition related variables based on observations at SMEAR I. Anthropogenic influence and uncertainties related to the used method are assessed as well. Finally in chapter 5, a summary of the thesis and concluding remarks are presented.

2. Background

2.1 Air Mass Classification

An air mass is a large, synoptic-scale body of air that has composition and meteorological characteristics typical for the surface below. As air masses are transported hundreds and thousands of kilometres by the wind field, they begin to adapt to the conditions of the new region. This transformation process changes the properties of the air mass via energy, moisture and mass fluxes from the surface and the surrounding regions. The change from an air mass type to another is not sharp and often happens in a time scale of days.

2.1.1 Traditional Method

Traditionally air masses are divided according to the latitude of region of origin, for example Arctic, polar and tropical. Additionally, air masses are often classified to be either continental (dry) or maritime (moist). This type of classification is known as the Bergeron classification (Bergeron, 1930) and is commonly used. The method is relatively easy to use because only temperature and moisture observations are needed. Moreover, to understand the dynamics of the atmosphere, temperature and moisture patterns are the key characteristics to understand, which makes the classification sensible.

2.1.2 Other Air Mass Properties

For some purposes, for example air quality studies, other properties of an air mass than temperature and humidity can be even more important. Concentrations of certain chemical compounds and ultrafine aerosol particles can be key characteristics when assessing health effects of ambient air (e.g. Peters et al., 1997; Kampa and Castanas, 2008). Both gases and aerosol particles also play a role in cloud processes (Kulmala et al., 2004), making them also important characteristics to understanding atmospheric processes from micro- to mesoscale. The concentrations of gases and aerosol particles are governed by their sinks and sources. They have varying atmospheric lifetimes depending on a wide range of factors, such as volatility of the compound, particle size, surface type and weather conditions.

Aerosol particles

An aerosol is a suspension of liquid or solid particles in a carrier gas. The diameter of these particles varies from about a nanometre to over hundred micrometres and they exist everywhere in the troposphere. Aerosol particles are often quantified according to their number concentration, mass concentration, particle size distribution and chemical composition. Several processes alter these properties continuously in the atmosphere. The effect of these processes on the properties mentioned above will be discussed in this section, with the exception of the chemical composition of aerosol particles, which is not studied in this thesis.

The size of an individual aerosol particle can be quantified using several types of characteristic diameters. One of the most commonly used diameters is the electrical mobility equivalent diameter, due to measurement techniques based on electric fields (e.g. (Aalto et al., 2001)). It is also the diameter referred to in this study when discussing the measured diameter. Particles are often divided into four modes in growing diameter ranges: nucleation mode, Aitken mode, accumulation mode and coarse mode. There are no standard diameter ranges used for these modes. In this study, the diameter ranges used for nucleation, Aitken, accumulation and coarse modes are <25 nm, 25-90 nm, 90-1000 nm and >1000 nm, respectively.

The nucleation mode includes particles formed in the nucleation process of low-volatility vapours (Kulmala et al., 2001). These particles are referred to as secondary aerosol particles and the formation process of these particles is known as atmospheric new particle formation (NPF)(Kulmala et al., 2004; Kerminen et al., 2018). The first clusters are typically less than a nanometre in diameter, and given suitable conditions, nucleation mode particles can grow into Aitken mode particles. Particles can grow by coagulation (collisions of particles) or condensation and the growth of particles is quantified by growth rate (unit nm h^{-1}). If particles grow large enough, approximately 100 nm in diameter, particles can act as cloud condensation nuclei (CCN)(Kerminen et al., 2005). Particle size can also decrease by evaporation, if the concentration of condensing vapours is low.

The number concentration of aerosol particles is the number of particles of any size in a volume of air, typically in a cubic centimetre. The particle number concentration in a volume of air increases either by direct emission of particles (primary aerosol particles) or by NPF. Primary particle emissions can be natural (e.g. pollen, sea salt) or anthropogenic (e.g. soot from combustion processes). The number concentration of aerosol particles decreases by coagulation and by deposition, either wet or dry deposition. Dry deposition is a rapid process for coarse mode particles (tens of micrometres in diameter) due to gravity and impaction (Schutz, 1979), and for nucleation mode (diameter of nanometres) due to Brownian diffusion (Ounis et al., 1991). Thus, the largest and the smallest particles

are not very effective tracers of air masses, but particles of the size range in between (Aitken, accumulation mode) can remain airborne much longer. Wet deposition is the other deposition mechanism and it means removal of both gases and aerosols from air by hydrometeors. In this way CCN, ice nuclei, gas molecules and particles are partially scavenged from the air. The processes that govern aerosol number concentration and particle size are summarised in Table 2.1.

Table 2.1: Key processes that alter aerosol number concentration and size of individual aerosol particles. Vapour concentration refers to the concentration of the nucleating or condensing vapour.

Process	**Effect on particle number**	**Effect on particle size**	**Effectivity mainly depends on**
Nucleation	increase	-	Vapour concentration
Condensation/ evaporation	-	increase/ decrease	Vapour concentration, particle size
Coagulation	decrease	increase	Particle concentration and size
Deposition	decrease	-	Particle size, surface properties

Quantifying aerosol properties can be done in many ways and each quantity has limitations. The problem in using the total number concentration as a characteristic value is that aerosol particles vary in diameter from less than a nanometre to tens of micrometres and particles at both ends of the scale have very different properties. Another way to measure aerosol amount is the mass of particulate matter (PM) below a certain diameter threshold. PM is a flawed measure as well due to ultrafine particles having very small contribution to the total mass, although they are of great importance for their negative health effects and role in microphysical processes.

The most insightful information to know would be the particle number size distribution which quantifies the relative importance of different size ranges contributing to the total concentration and mass. Particle size distribution is a two-dimensional (diameter and concentration) quantity, so it is sometimes not a convenient measure. Condensation sink (CS) is a simplified aerosol quantity describing the sink of vapours to the particle phase (unit s^{-1}). CS strongly depends on the size distribution of particles, as large particles are weighted more than smaller particles (Equation 2.1).

$$\begin{aligned} CS &= 2\pi D_v \int_0^\infty d_p \beta_M(d_p) dd_p \\ &= 2\pi D_v \sum_i \beta_{M_i} d_{p,i} N_i \end{aligned} \tag{2.1}$$

where:

D_v = vapour diffusion coefficient
d_p = particle diameter
β_M = transitional correction factor for particle
N = number of particles

If CS is high, the population of particles is effective in consuming vapours by condensation. The inverse of CS describes the lifetime of a vapour molecule with the properties of sulphuric acid and zero saturation vapour pressure at the surface (irreversible condensation).

Atmospheric trace gases

The dispersion area extent and spatial concentration variability of a gas greatly depends on the atmospheric residence time of the gas. Atmospheric residence time is defined as the average time a molecule spends in the atmosphere before it is removed via deposition or chemical reaction. Inert gases such as argon (Ar) or nitrogen molecule (N_2) are long-lived and well mixed in the atmosphere and thus bad air mass tracers. However, many atmospheric gases have a residence time of hours, days or weeks, which means they are only transported some hundreds or thousands of kilometres before their removal from the atmosphere. These gases are called trace gases and they make up only a minor portion of the total mass of the atmosphere.

If a trace gas has a residence time of at least several days or weeks, it can have a relatively high background concentration, which means the concentration in absence of local sources. If the atmospheric residence time of a gas is short (hours or less), it is a good tracer of local sources. The most relevant trace gases to study, due to their negative health effects and important role in NPF events, are sulphur dioxide (SO_2), nitrogen oxides (NO_X), carbon monoxide (CO) and ozone (O_3). Here, the unit used to express the concentration of these gases is parts per billion (ppb).

The tropospheric residence time of SO_2 is typically 1-2 days (Barrie and Hoff, 1984), so it can be transported up to thousands of kilometres from the emission source. It is emitted to the atmosphere mainly in combustion processes of fossil fuels and volcanic eruptions. In remote marine areas like the Arctic, phytoplankton has a relatively large contribution to SO_2 and particles via dimethyl sulphide (DMS) production (Yang et al.,

2016; Park et al., 2017). This is a particularly important mechanism during the summer months because DMS is mainly oxidised to SO_2 by the hydroxyl radical, which is a daytime product (Keller, 1989). SO_2 is a precursor gas of sulphuric acid (H_2SO_4), which is the single most important compound contributing to early stages of NPF (e.g. Yao et al., 2018).

N_2 is the most abundant gas in the atmosphere and is stable due to its triple bond. At high temperatures the bond can break, which allows the nitrogen atom to be oxidised into NO_X. NO_X consist of both nitrogen monoxide (NO) and nitrogen dioxide (NO_2) and they are the most reactive of the studied trace gases. Combustion processes are the most important source of NO_X, but natural sources also exist, from e.g. lightning strikes. Due to a rapid reversible reaction with ozone, the concentrations of NO and NO_2 fluctuate but their combined concentration is more stable, hence the concentration NO_X is a commonly used air quality characteristic. Due to the complexity of NO_X reactions, their lifetime varies roughly from 2 to 8 hours depending on the emission strength, wind conditions and background chemistry (Liu et al., 2016).

Ozone is produced in photolytic reactions from its precursor gases: methane, CO, volatile organic compounds (VOCs) and NO_X (Monks et al., 2015). Most of it is in the stratosphere, where ultraviolet (UV) radiation is available for production. A fraction of UV radiation makes it to the troposphere, allowing small concentrations of tropospheric ozone to be formed. Ozone can also be transported from the stratosphere to the troposphere (Oltmans, 1981). The residence time of tropospheric ozone varies from weeks in rural environments and the free troposphere, to hours in urban, polluted environments where reactive compounds are available. Thus, tropospheric ozone is relatively well mixed in marine and polar environments, which are generally only moderately polluted.

CO has a tropospheric residence time of about a month - long enough for long distance transport but not long enough to be evenly mixed in the atmosphere (Weinstock, 1969). Wildfires and volcanoes are examples of natural sources of CO. Anthropogenic sources include motor vehicles, industrial activity and domestic heating.

The concentrations of all of the aforementioned trace gases are affected by incoming solar radiation. The most significant oxidant of SO_2, NO_X and CO is the hydroxyl radical ($\cdot$OH), which is photochemically formed (Arakaki and Faust, 1998). In winter months other processes, such as dry deposition, become relatively more important, but the sinks are not large enough to balance the sources. Thus, especially the seasonal variation in the concentrations of the longer-lived gases of CO and O_3 is characterised by a winter maximum and summer minimum (Vingarzan, 2004). The annual net flux to the atmosphere is nearly zero, although a weak increasing trend in the concentration of CO has been observed, which is likely of anthropogenic origin (Khalil and Rasmussen, 1990). A summary of the properties of the gases analysed in this study is shown in Table 2.2.

Table 2.2: Properties of the tropospheric trace gases examined in this study. The residence times and typical concentrations are only rough estimates and show large variation globally. The unit used for the concentration is parts per billion (ppb).

Tropospheric trace gas	**Tropospheric residence time**	**Main sources**	**Main sinks**	**Typical tropospheric conc. (ppb)**
Sulphur dioxide, SO_2	1-2 days	Volcanic Eruptions, oxidation of DMS, fossil fuel burning	Oxidation to sulphate aerosol or H_2SO_4	0.01 - 10
Nitrogen oxides, NO_X	2-8 hours	Lightning, combustion processes	Atmospheric oxidation	0.01 - 10
Carbon monoxide, CO	1-2 months	Wildifres, combustion processes	Atmospheric oxidation, soils	100 - 1000
Ozone, O_3	hours to weeks	Production by solar radiation, stratospheric transport	Photochemical destruction, dry deposition	10 - 100

An important group of gas compounds for the NPF processes is VOCs (Laaksonen et al., 2008). These vapours have a low volatility, so they have a higher probability to remain in a liquid phase after condensation. Thus, the lack of VOCs is often the barrier for NPF events. There are numerous organic gases that belong to VOCs and they are known to be emitted from both anthropogenic (e.g. combustion processes, Tissari et al., 2008) and biogenic (e.g. vegetation, Hakola et al., 2012) sources. Biogenic VOCs in the boreal environment are mostly emitted to the atmosphere in the presence of solar radiation. They are good tracers of air masses due to their multiplicity, but understanding the complexity of them is often limited and identifying them from an air sample requires sophisticated instrumentation. Hence VOCs are not analysed in this study.

2.1.3 Arctic Air Mass Characteristics

Arctic air masses are colder and typically have a lower moisture content than polar air masses, although the difference is less pronounced in winter (Curry, 1983). Arctic air masses develop in the high northern latitudes that are, to a large extent, covered by sea ice or the ice sheet of Greenland. This is why Arctic air masses are typically continental, although there is large seasonal variation in the sea ice extent, as shown in Figure 2.1. The region north of Scandinavia remains open from ice all year round, allowing large fluxes

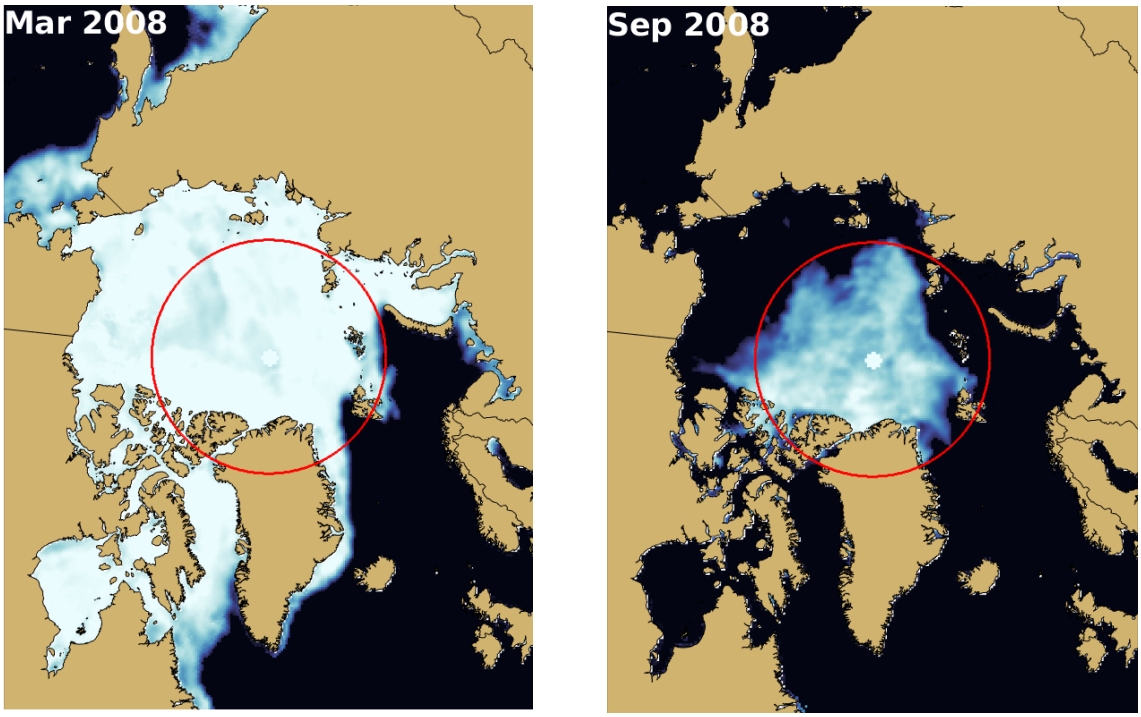

(a) Spring maximum **(b)** Autumn minimum

Figure 2.1: The sea ice concentration for spring maximum and autumn minimum in 2008, which here represents an average year in the 1998-2017 time period. Bright colour means high sea ice concentration and dark colour represents open sea surface. The red circle illustrates the 78th parallel north, which was used as the boundary for air masses to be classified as Arctic (further explained in section 2.2). The sea ice concentration data was obtained from the National Snow and Ice Data Center (Maslanik and Stroeve, 1999).

of latent and sensible heat at the sea surface to modify the air mass properties. Hence, initially continental Arctic air masses spend tens of hours over open sea before they can reach the coast of Norway or Russia prior to arrival in Finland.

What makes the Arctic (and the Antarctic) region special is that it is practically uninhabitated by humans. This means that there are no major, local sources of anthropogenic pollution. Because vegetation is very limited in the region, biogenic sources are weak as well, especially in winter. If an air mass develops over an open-sea surface, primary particles are emitted to the air in presence of wind-induced sea spray. Sea salt particles are large in diameter (typically > 1 μm) and thus have a short atmospheric residence time, which makes it unlikely they will be transported deep into continental areas before their removal from the air by dry deposition. The wet deposition mechanism is also enhanced in maritime Arctic environments (Mauritsen et al., 2011).

Low temperature and relative humidity and the absence of pre-existing particles (low CS) are favourable conditions for a NPF event (Nilsson et al., 2001), but Arctic air masses are also void of necessary gases that can initiate the nucleation process. This is

the reason why Arctic air masses are often a good base for NPF (Sogacheva et al., 2005), as soon as the air spends enough time overland for biogenic emissions of volatile organic compounds (VOC) to allow growth of ultrafine particles towards CCN size (Väänänen et al., 2013).

There is no commonly used source region for Arctic air masses in literature, and defining such boundaries would be difficult, as the Arctic front, which separates the air masses, keeps changing its shape. An estimate of its location based on the average location of the surface level -5 °C isotherm in summer and winter, as suggested by Li et al. (1993), is given in Figure 2.2a. Their definition is likely to include continental polar air masses to also be defined as Arctic air masses in winter. A more straightforward approach has been taken by the International Maritime Organization (IMO) in Figure 2.2b, who defined the boundary to be north of 60 °N with the exception of the ice-free region around Iceland and the coast of Norway (Jensen, 2007).

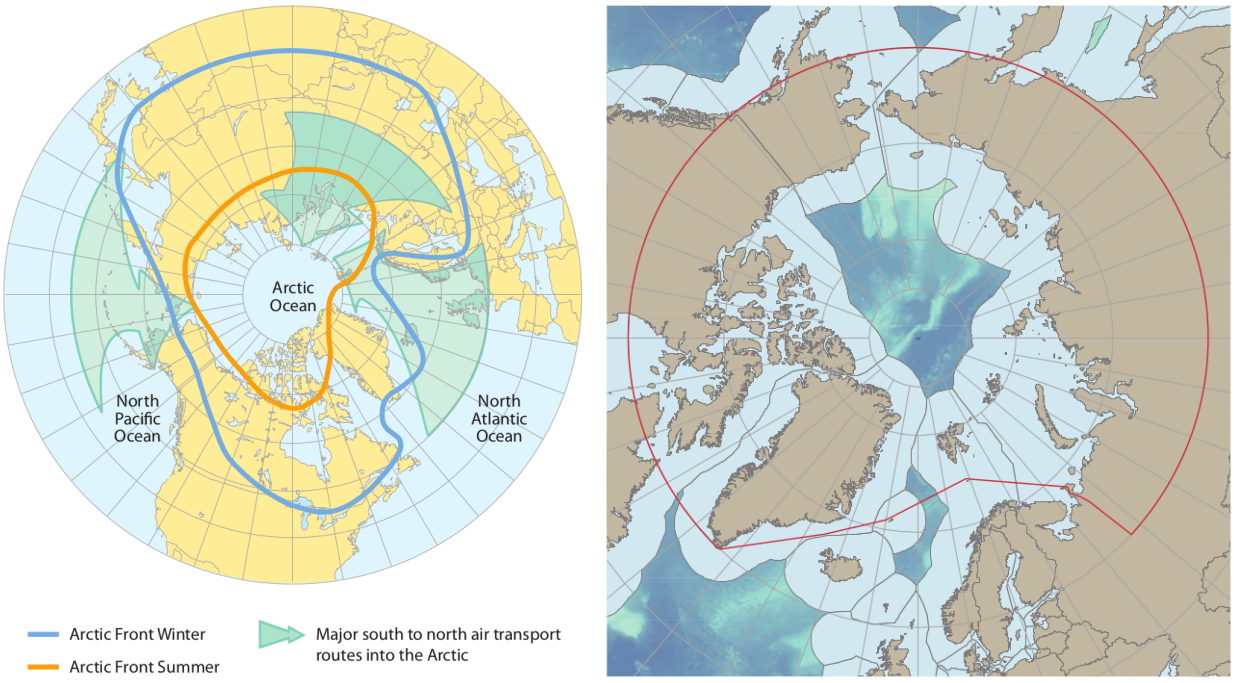

(a) Arctic front position (Li et al., 1993)

(b) Arctic area (Jensen, 2007)

Figure 2.2: Two different ways to estimate the Arctic region extent: a) from mean meteorological conditions and b) from sea ice extent (IMO). Figures are adapted from the original publications by AMAP (2015).

Mixed layer height is also a variable to consider when analysing changes of Arctic air mass properties in time. The mixed layer is a type of planetary boundary layer; it is defined to be the layer in contact with the surface that is well mixed regarding energy (heat, momentum) and mass (particles, trace gases) in the vertical direction (Stull, 1988). The height of it varies from tens of metres in stable winter conditions to several kilometres

on a sunny summer day. The mixing occurs primarily by thermal and mechanical turbulence, and the magnitude and relative importance of these two types of turbulence vary diurnally, seasonally and regionally. Thermal turbulence is generated by radiative heating at the surface, so it is weak at night and in winter due to minimal solar heating and in marine environments due to the high heat capacity of water compared to the continent. Mechanical turbulence is generated by wind shear, which is caused by surface roughness and the logarithmic vertical wind profile due to friction at the surface. Mechanical turbulence generation is usually weaker over a water surface due to low surface roughness, but on the other hand wind shear can be strong due to high wind speeds because friction is lower than over continents. As Arctic regions are cold and have usually a smooth surface, the mixed layer height is typically less than 250 metres (Nilsson, 1996).

2.2 Atmospheric Trajectories

An atmospheric trajectory is the path of an air parcel as it is advected by a wind field in time. A forward trajectory is the path forward in time, a backward trajectory in turn describes the movement of the air parcel before it arrives at the point of interest (e.g. a measurement station). Forward trajectories can be useful when assessing the impact of point-like emission sources. For example, spreading of volcanic ash or radioactive fallout can be estimated by using forward trajectories (Stunder et al., 2007; Lozano et al., 2011). Backward trajectories can be useful when trying to explain changing conditions in a certain place, a measurement station for example (Sogacheva et al., 2005). The latter approach has been taken in this thesis to examine the properties of arriving Arctic air masses.

It is obvious that calculating trajectories with an accuracy of metres for just several hours would require unrealistic computational resources, knowledge of the initial state and understanding of physical processes governing the transport. Yet, trajectories can be calculated to obtain an estimate of air particle transport in scales of kilometres. The uncertainty related to atmospheric trajectory calculations has been assessed by Stohl (1998). He estimated that the horizontal error is in the order of 20 % of the distance traveled. The accuracy of the trajectory output of a model depends on the model itself (e.g. how well are physical processes modeled) and the meteorological gridded dataset that is required as input.

It can be assumed that air masses transported from the high northern latitude region are Arctic in nature. Making this assumption allows the identification of Arctic air masses to be done from backward atmospheric trajectories by examining the source latitude a certain number of hours before arrival. This method may not be very accurate for identification of other (e.g. tropical) air masses, because there is more zonal variation

of air masses in the midlatitudes.

In this study, Arctic air masses are defined to be those originating from latitude 78° N or higher, 72 hours before arrival at a measurement station in Värriö. This criterion was defined after sensitivity testing using latitude limits from 70° N to 83° N. Overall, Arctic air mass observations of all months steadily declined from 38 % Arctic fraction to 7 % when the latitude criterion was increased, which corresponds to approximately 2.4 % decrease per degree of latitude.

The threshold of 78° N was chosen as it is a high enough latitude to make sure that the air is Arctic, but low enough to have sufficient data even in summer months, especially July, to make a meaningful interpretation of results. The goal was to capture cases where air masses are transported along a more or less direct route to Värriö. Using this threshold, the shortest distance to the station from what was defined as the Arctic, is almost 1100 kilometres. To be transported this distance in 72 hours, the minimum average wind speed required is 4 m s^{-1}. This means that it is likely that air masses that are classified as Arctic have only been minimally modified over land areas below the 70th parallel north.

Atmospheric trajectory data can also include information of the height of the mixed layer at each position, obtained from the gridded meteorological dataset. Whether the air parcel is in the mixed layer is valuable information because it determines how strongly surface phenomena, such as heat, moisture and mass fluxes are affecting the parcel. Hence, air parcels that are not in the mixed layer are expected to have lower aerosol particle and trace gas concentrations, if the emission sources are at the surface.

3. Data

3.1 Trajectory Data (HYSPLIT)

To calculate backward atmospheric trajectories, the Hybrid Single Particle Lagrangian Integrated Trajectory (HYSPLIT, Stein et al., 2015) model was employed, which is a widely used trajectory model for calculating forward or backward atmospheric trajectories. HYSPLIT has been developed for over 30 years and the version used here is version 4 (Draxler and Hess, 1997). Several optional features can be included in the model, such as pollution dispersion or vertical motion following isentropic or isobaric surfaces. For this study, a simple single-particle trajectory mode was chosen with the vertical velocity obtained from the vertical motion field of the meteorological gridded data. Horizontal transport is calculated from the horizontal wind field that advects the air parcel.

The meteorological gridded datasets used for this study are produced by the National Weather Service's (NWS) National Centers for Environmental Prediction (NCEP). Two datasets were used in this study. From 1998 to 2006 the used product was Final Operational Analysis Data (FNL), which is the final product in operational use produced by NCEP. During the study period, the horizontal resolution of the NFL data was 191 km with 13 vertical levels and the temporal resolution was 6 hours. From 2007 to 2017, a higher resolution Global Data Assimilation System (GDAS) meteorological dataset was used at 1x1-degree (110x110 km) horizontal resolution with 23 vertical levels and at 3-hour temporal resolution. If HYSPLIT is run at a higher temporal resolution than the meteorological gridded dataset used as input, linear interpolation is used by the model.

Trajectories were calculated backwards for 72 hours with a 1-hour temporal resolution using 100 m arrival level above SMEAR I. The low arrival level was chosen to best represent conditions measured at the surface. The output trajectory files, along with the coordinates (latitude, longitude, altitude), also included potential temperature of the air parcel and mixed layer height at the current position at each time step.

3.2 SMEAR I

3.2.1 Station Description

Station for Measuring Ecosystem-Atmosphere Relations (SMEAR) is a station concept designed to measure a wide range of atmospheric and biospheric variables in the long term (Hari et al., 2016). There are four SMEAR stations in Finland, one in Estonia and one in China. SMEAR I in Värriö (67°46'N, 29°36'E, 390 m above sea level), in Finnish Lapland, was the first one to be built (Hari et al., 1994). The first long-term measurements of several atmospheric gases began in 1992, but a more comprehensive set of variables, including the particle size distribution, has been continuously measured since 1997.

SMEAR I is located in a very sparsely populated area in close proximity to the Värriö fjeld range, pine forest and swamps. The canopy height is less than 10 metres (mean height 6.7 m, Hari and Kulmala, 2005). The station is not located on flat land, therefore temperature inversions and local wind patterns, such as katabatic winds, might make local measurements of wind unrepresentative of the large-scale flow. Due to the northern location, incoming solar radiation is very weak from October through February. The polar night lasts for over two weeks, from December 13th to December 31st. The snow depth can exceed one metre during winter months.

Two major mining industry sites are located nearby, in the Kola Peninsula: Nikel (69°25'N, 30°15'E) to the north and Monchegorsk (67°55'N, 32°50'E) to the east of SMEAR I, which are 188 and 146 kilometres away, respectively (Figure 3.1). Highly polluted air is frequently transported to Värriö from these industrial sites (e.g. Vehkamäki et al., 2004; Kyrö et al., 2014). The distance to the Arctic Ocean is 230 km and to the Russian border 6 km.

3.2.2 Station Measurements

Instrumentation changes have taken place for many of the instruments over the years. A full list of instruments and times of installation is available online at SMEAR Wikispace (Aalto, 2017). Initially measurements were taken at several vertical levels for many variables. Most of the measurements are currently taken from a single level per measured variable: air temperature and pressure at 2 m, gases and humidity at 9 m, radiation at 16 m and particles near the surface, below the canopy height. Tree growth and gas exchange are measured directly from individual trees at the station site.

Meteorological observations that were used for this study include measurements of temperature, humidity (dew point temperature), atmospheric pressure, precipitation and

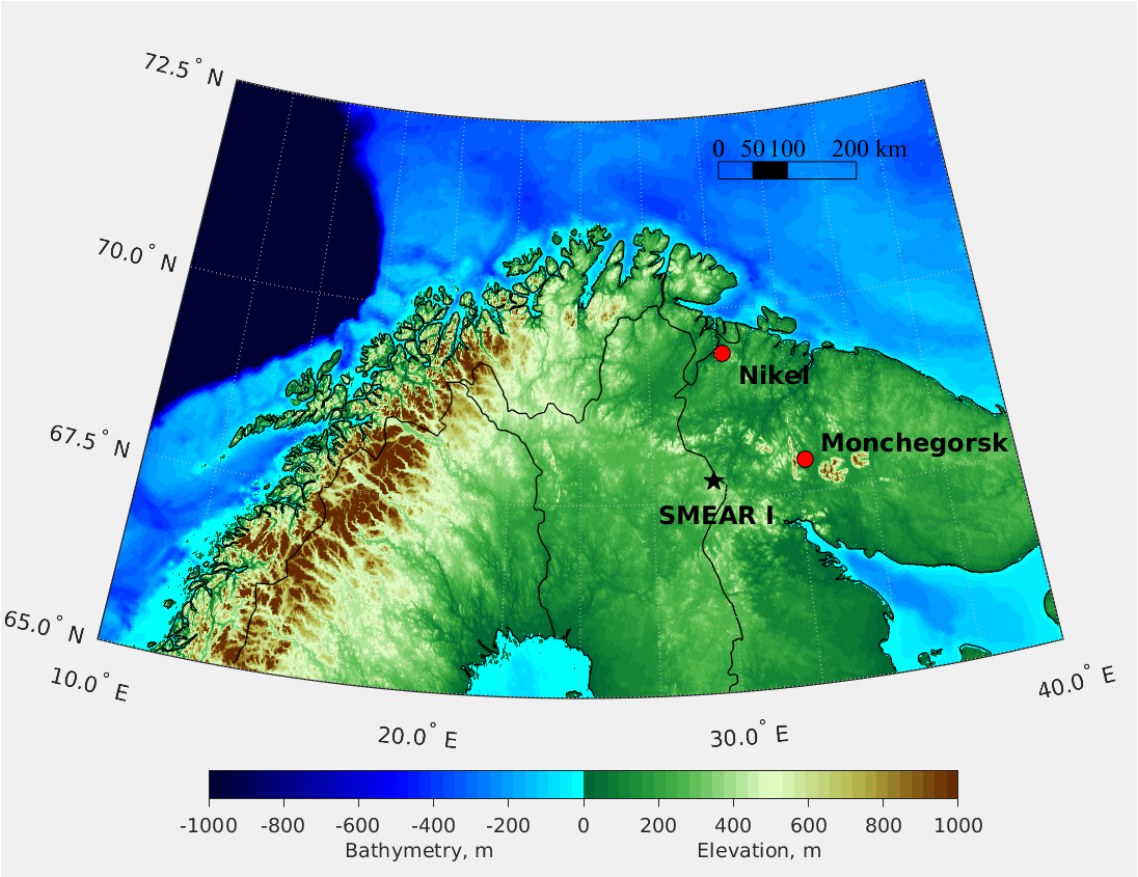

Figure 3.1: Map representation of topography and bathymetry in the region where SMEAR I is located. The two largest pollution sources, Nikel and Monchegorsk, are marked with red markers.

irradiation. The temporal resolution of the measurements of meteorological variables has changed several times. It was 20 min for the measurements of temperature, pressure and humidity until April 2009, when it was increased to 1 min. Irradiation was initially measured at a 5-minute temporal resolution, which was increased to 1 min in May 2011. The measurements of liquid precipitation also had original temporal resolution of 5 minutes, which was increased to 1 min in 2011. Year-round precipitation has been measured since April 2008, and the temporal resolution used has been 1 min except for the time between April 2009 and January 2010, when it was 5 minutes.

Precipitation has been measured using two fundamentally different measurement instruments with different limitations. Liquid precipitation has been measured using a traditional tipping-bucket type rain gauge since the beginning of the study period, but its use is limited to the warm season only (roughly from May through October). The rain gauge can only measure each 0.2 mm of rainfall, thus it is possible that it is not able to record very light rain accurately (Habib et al., 2001). A laser disdrometer was installed in 2008 to allow precipitation observations in winter as well, and with overall lower detection limit (0.01 mm min^{-1}). Most, although not all, uncertainty related to

the optical disdrometers can be avoided by regular calibrations (Moraes Frasson et al., 2011). Tipping-bucket rain gauges tend to underestimate and optical disdrometers tend to overestimate rainfall accumulation at heavy rain rates (Tapiador et al., 2012), but heavy rainfall is not typical in the high-latitude climate of Värriö. In this study, the observations of the optical disdrometer have been used and the results of a comparison of the two instruments are presented in section 2.4.3, where precipitation results are discussed.

The particle number size distribution is measured at SMEAR I using a Differential Mobility Particle Sizer (DMPS). The DMPS system consists of a Differential Mobility Analyzer which separates a certain size range of particles from the input flow and a Condensation Particle Counter (CPC) which counts the particles directed to it by the DMA (Aalto et al., 2001). During the first six years (1997-2002) only one DMA with a classification limit of 10 nm was taking measurements. Another DMA/CPC pair was added in spring 2003, after which the installation setup has been able to detect particles down to 3 nm diameter. The temporal resolution of the DMPS measurements was 10 min for the whole study period.

The trace gases analysed in this study were SO_2, NO_X, CO (since 2010) and O_3. The temporal resolution of the trace gas measurements was 10 min in 1998-2009 and 1 min thereafter. In principle, to measure the concentration of NO_X, individual measurements of NO and NO_2 are needed. The concentration of NO_2 has not been directly measured before 2016, instead the concentrations of total reactive nitrogen NO_Y and NO have been measured. NO_Y consists of NO_X and minor concentrations of other forms of oxidised nitrogen (e.g. nitric acid and peroxyacyl nitrates). In this study it is assumed that the concentration of other nitric compounds than NO_X can be neglected and therefore NO_Y is referred to as NO_X. The detection limits of the instruments used to measure concentrations of SO_2, NO, NO_X, O_3 and CO were 0.02 ppb, 0.1 ppb, 0.1 ppb, 1 ppb and 20 ppb, respectively.

The data coverage for the study period 1998-2017 was good for almost all of the variables included in the analysis (Figure 3.2). Precipitation has only been measured for the warm season until 2008. Apart from that, the data used in this study had temporal data coverage above 95 % for meteorological variables and above 85 % for gas and particle measurements since installation. Short breaks in the data are caused typically by changes in the instrumentation and maintenance breaks.

3.3 Data Processing Steps

Most of the SMEAR data were downloaded from the Smart-SMEAR AVAA portal (Junninen et al., 2009). Gas data from 1999 and 2001, inverted DMPS distribution files and

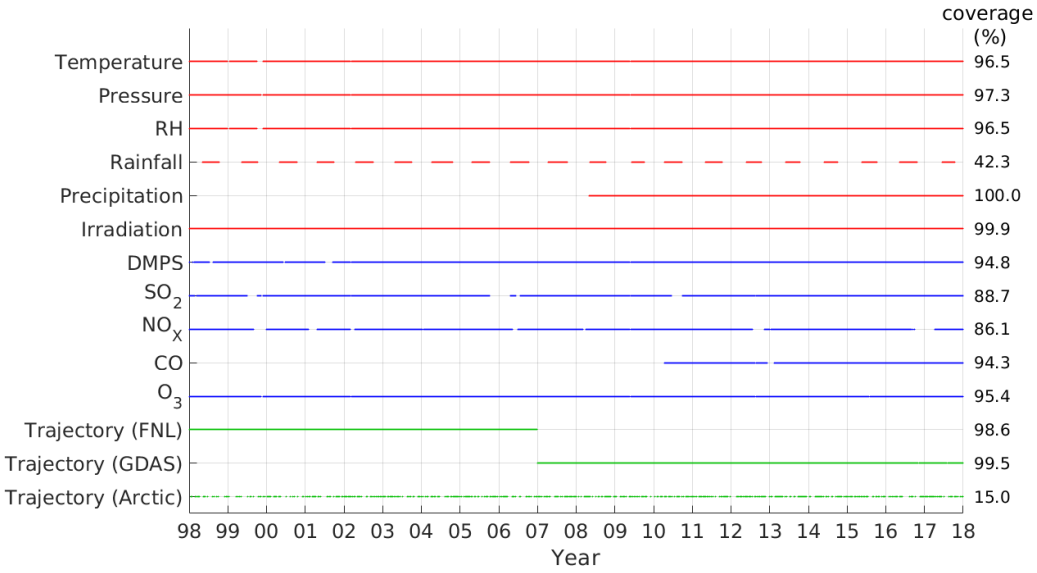

Figure 3.2: Temporal coverage of quality-checked measurements in 1998-2017 at SMEAR I. Only variables that have been relevant to this study have been included. Meteorological variables are shown in red, particle and gas related variables in blue and trajectory availability in green. Coverage percentage is calculated based on the first available data point for each variable. "Rainfall" refers to liquid precipitation, and "Precipitation" to liquid and solid precipitation.

trajectory files were directly downloaded from a local server. All data were converted to the same time zone (UTC) and averaged to one-hour resolution. For most of the variables considered here, the averaging method used was the median and not the mean, to minimise the effect of individual outliers in the data. Rainfall was converted to hourly resolution using the sum of all data points in an hour to obtain the unit of rain rate in mm h^{-1}.

A slightly different procedure was needed for the DMPS data. The number of channels in the DMPS instrumentation has changed several times over the years. Thus, the detection range (3-1000 nm) was divided into 50 size bins uniformly distributed on a logarithmic scale. After interpolation to these size bins, the median value in each size bin was taken separately for every hour of data to obtain a temporally averaged size distribution.

After averaging the trace gas data, the units were converted from μg m^{-3} to parts per billion (ppb). As the concentration of NO is so low compared to that of NO_2, molar mass of NO_2 was used in unit conversion of NO_X. After hourly averaging, values that were below the corresponding detection limit for each gas were set to half of the detection limit in attempt to avoid underestimation of the concentrations. This frequently occurs with the measurements of SO_2 and NO, because their background concentrations are typically very low in Värriö.

The trajectory files were analysed to create a list of hours when the latitude criterion

was met (78° N, 72 hours before arrival at SMEAR I). This list was used to separate those lines of SMEAR data that were classified as associated with an Arctic air mass. As a result, two datasets were obtained: one with hourly data points that were classified as Arctic and the remaining data points which is referred to as the non-Arctic dataset. The trajectory data was also used to analyse typical paths of Arctic air parcels. For this purpose, Earth was divided into half-degree grid cells and the frequency each cell was visited at any hour by a trajectory was calculated. This was repeated for all Arctic air mass trajectories and the counts were converted into percentages. Data processing steps are illustrated in Figure 3.3.

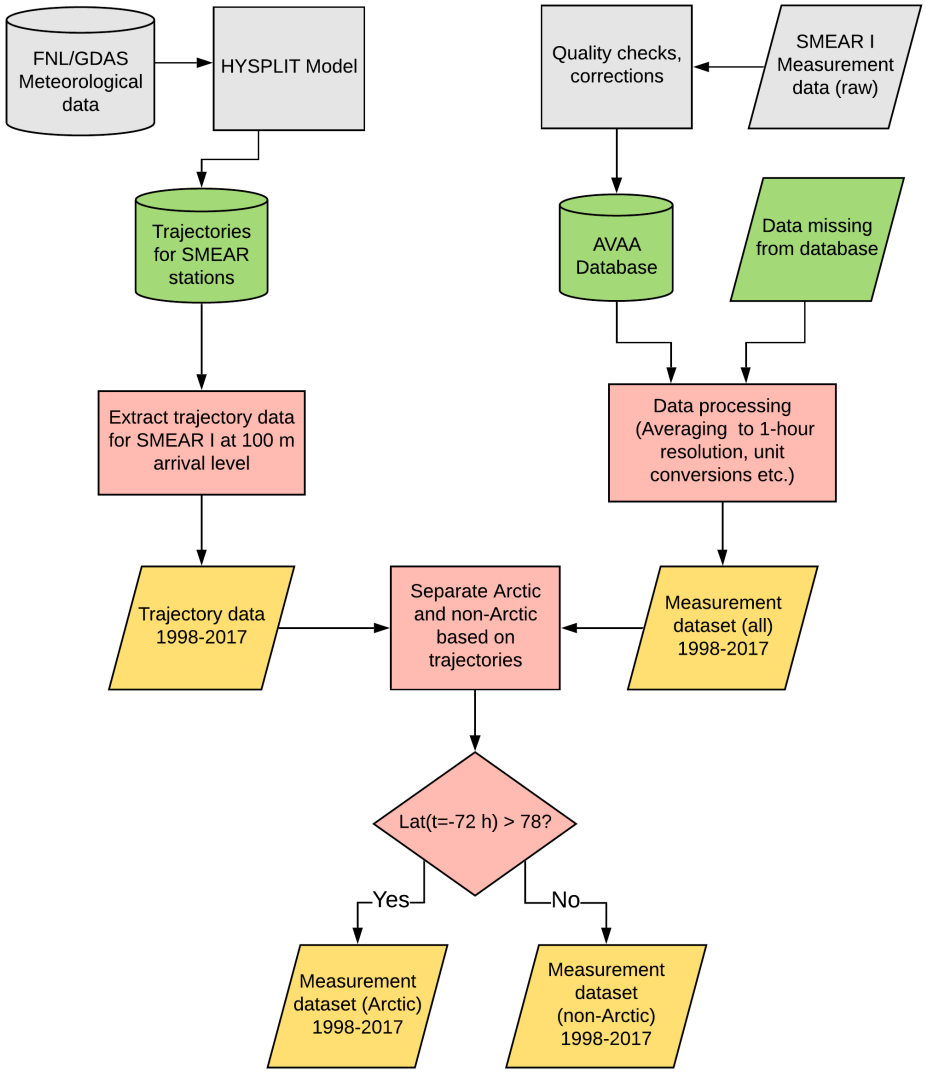

Figure 3.3: Data processing steps. The data products that were available as starting point of this study are marked in green colour, and the steps necessary to provide those data in grey. The end products of this study are marked in yellow colour and the red objects mean data processing steps.

4. Results and Discussion

4.1 Trajectory Statistics

Overall, 15.0 % of all hours in 1998-2017 were classified as Arctic based on the trajectory analysis using the threshold that requires a trajectory to be north of 78° N, 72 hours before arrival at SMEAR I. This corresponds to 55 days per year on average. The mean distribution of monthly Arctic air mass occurrences is shown in Figure 4.1. The average total duration of Arctic events per month was the highest in March (7.5 days) and the lowest in July (2.0 days). The fraction steadily increased in autumn, but decreased in January (4.6 days) and February (3.5 days). More than one third of the observed Arctic air mass conditions took place in spring months (March-April-May). The inter-annual variation in the total duration of Arctic air mass events in a month was large in all the seasons.

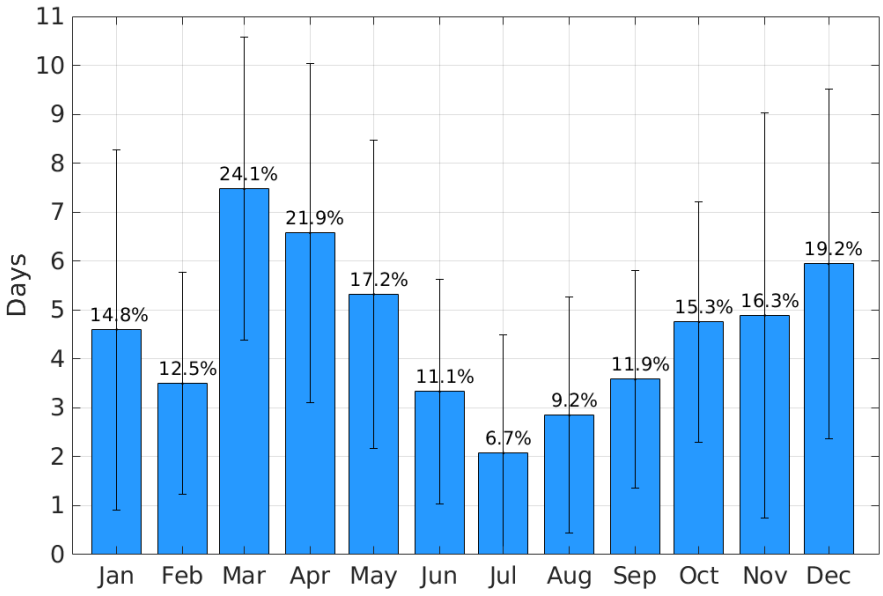

Figure 4.1: The mean total duration of Arctic air mass events per month. An air mass was defined Arctic if the 1-hour resolution backward trajectory placed it at latitude 78° N or higher 72 hours prior to arrival at SMEAR I. A cumulative sum of Arctic event duration was calculated for each month in 1998-2017 and then averaged to obtain an average monthly value. Duration is shown in days, even though individual events were typically shorter. The errorbars represent one standard deviation from the mean value and the percentages are the total duration divided by the number of days in each month.

Typical Arctic event duration was also studied (Figure 4.2). The longest period that was classified as Arctic occurred in December 2001 and lasted for 147 hours, and during the 1998-2017 period the mean duration was 18.5 hours and the median duration was 10.0 hours. A vast majority of the events lasted for less than two days and events longer than four days occurred on average less frequently than once a year.

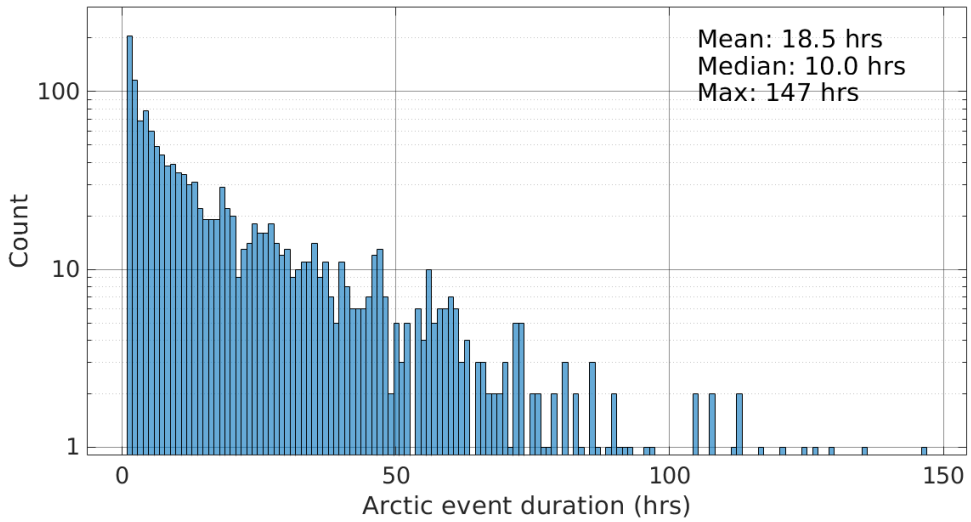

Figure 4.2: Histogram of the durations of individual Arctic air mass events at SMEAR I, Värriö, in 1998-2017 based on HYSPLIT analysis. Event duration was defined to be the sum of consecutive hours when the backward trajectories placed the air parcel 78° N or higher 72 hours prior to arrival at SMEAR I.

The typical seasonal trajectory paths in Figure 4.3 show two main paths for arriving Arctic air masses: one west of Svalbard (pathway 1) and one east of it (2). Pathway 2 is further divided to two branches: northern (2a) and north-eastern (2b). It is likely that the trajectories of pathway 1 have to ascend several hundred metres to cross northern parts of the Scandinavian mountains. The eastern branch is more prone to the Kola Peninsula influence, especially in months between June and August, when pathway 2b becomes more frequent (Figure 4.3c).

Both of the main branches are cyclonically curved, which suggests that Arctic air mass transport to Värriö is typically associated with low pressure systems that reach the region north-east or east of Värriö. This hypothesis is also supported by the short duration of individual Arctic air mass events, as shown in Figure 4.2.

As both the air parcel height and the thickness of the mixed layer at each time step were available in the trajectory data, the number of hours that each air parcel spent in the mixed layer along the 72-hour trajectory was determined. This analysis was only done for the Arctic air masses. A histogram of the results is shown in Figure 4.4, separately for the warm (May through October) and the cold (November through April) seasons.

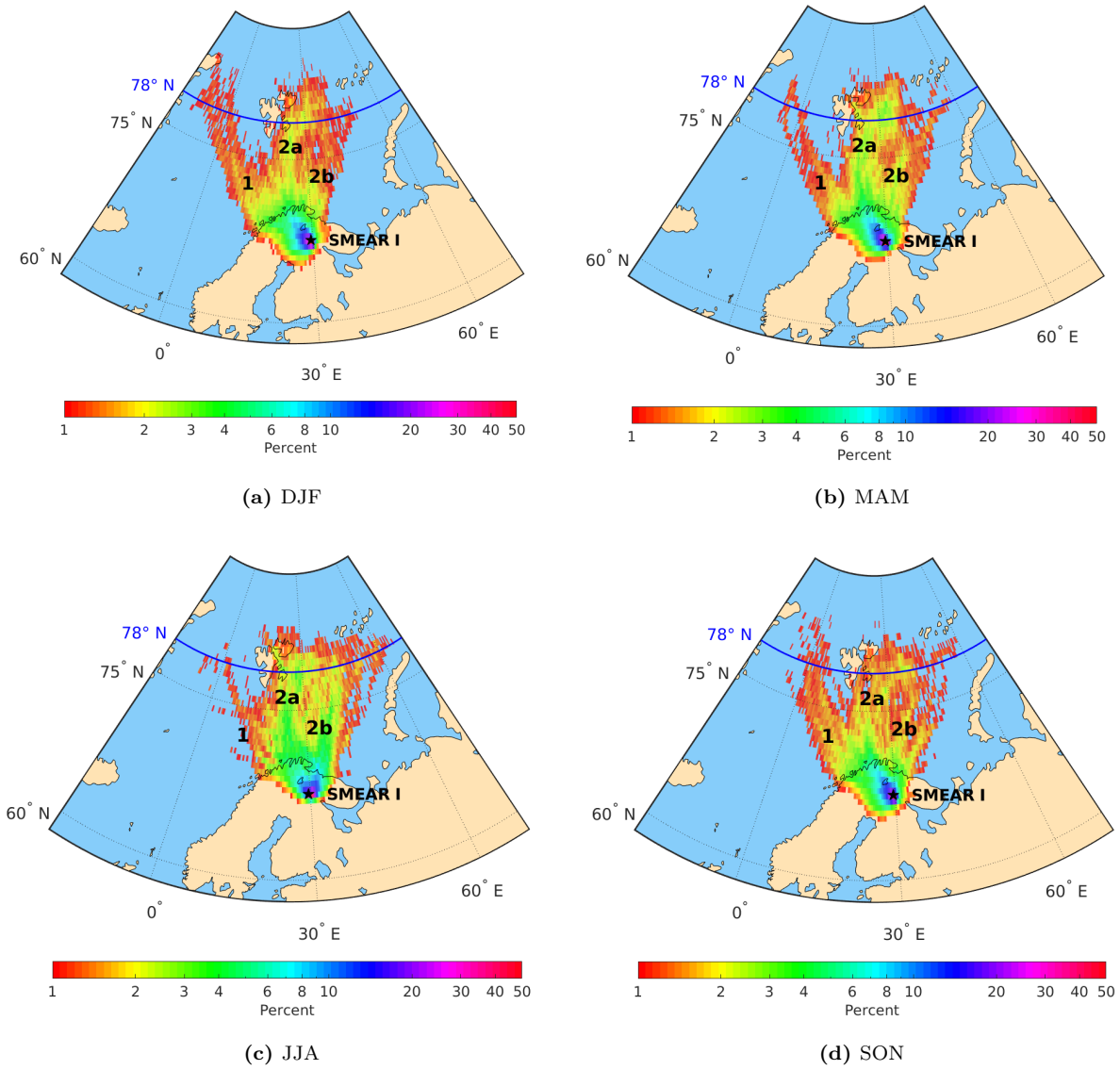

(a) DJF

(b) MAM

(c) JJA

(d) SON

Figure 4.3: Percentage of arriving Arctic air masses that have passed each 0.5 x 0.5 degree grid cell as they arrive at SMEAR I in a) winter (DJF), b) spring (MAM), c) summer (JJA) and d) autumn (SON). Pathways 1, 2a and 2b represent the most frequent pathways of air parcels. The analysis is based on HYSPLIT backward trajectories in 1998-2017. The Arctic air mass classification method is explained in section 2.2.

In the warm season over half (51.3 %) of the trajectories spent all 72 hours in the mixed layer and only 12.0 % of the trajectories spent less than two thirds (48 hours) of the time in the mixed layer. The corresponding values were 23.3 % and 30.9 % in the cold season. The median altitude of the trajectories along the path was also calculated and, averaged 83 metres in the warm season and 82 metres in the cold season. Thus, it can be concluded that the higher mixed layer residence time in summer is connected to the seasonal variation in the height of the mixed layer, not to seasonal differences in the trajectory paths.

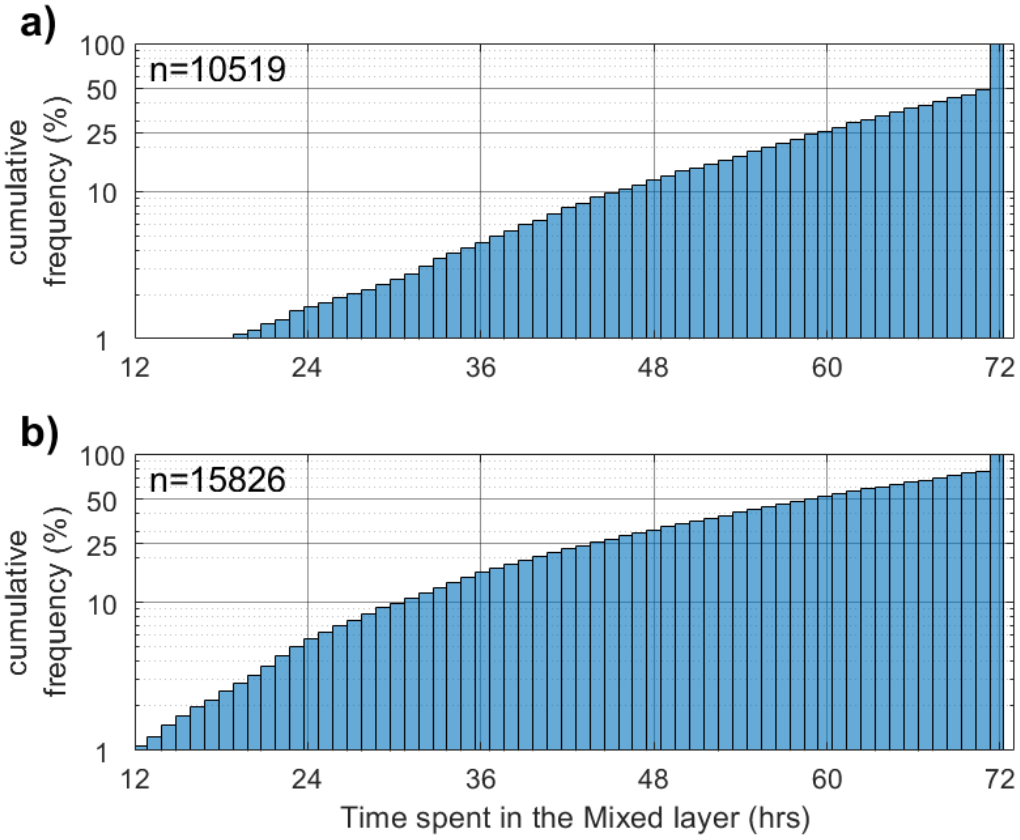

Figure 4.4: Histogram of the time individual 72-hour trajectories spend in the mixed layer for a) the warm season (MJJASO) and b) the cold season (NDJFMA). Analysis is based on HYSPLIT backward trajectories that were poleward of 78° N 72 hours before arrival at SMEAR I in 1998-2017. The arrival height of the trajectories was set to 100 m.

4.2 SMEAR I Observations

To analyse the seasonal or monthly variation of variables, figures of average conditions during a "median year" were constructed. This was done by dividing each year into 36 periods of approximately 10 days, and calculating a median value for those time periods (e.g. January 1st to January 10th) in 1998-2017 separately for the Arctic and non-Arctic datasets. The 25 and 75 % quartiles were also calculated to see the variability of the data, and in the rest of the chapter the shading in figures indicates the area between the quartiles. Quartiles were chosen instead of standard deviation because most of the variables examined in this thesis are not normally distributed and because the median, rather than the mean, is usually shown.

Statistical tests for the Arctic and non-Arctic datasets were not performed in this study for several reasons. Firstly, the seasons have drastic differences and hence testing a full year of data might not reveal statistically significant correlation, even if there is in fact a correlation within one season only. Secondly, the number of variables that were analysed

was quite large. The aim of this study is to give an overview of how different variables vary in Arctic and non-Arctic air masses, and how they might vary seasonally. Further studies could narrow down the focus on certain variables and seasons for statistical testing, based on this study. Thirdly, statistical tests for a particle size distribution would be difficult to perform. A solution could be to study the different modes or CS separately, but that would require extensive work.

4.2.1 Meteorology

Temperature, air pressure and wind

The median year of temperature variation is shown in Figure 4.5a. The temperature of the Arctic air masses was lower than in the non-Arctic air masses during most of the year. The difference was particularly pronounced in summer (5.6 °C in June-August), but was less clear in winter (2.0 °C in December-February). The temperature variability was also smaller for the Arctic air masses than for the non-Arctic air masses, which suggests that Arctic air masses are a more homogeneous subset.

The differences in air pressure between the datasets were small, and especially the Arctic air pressure data were noisy (Figure 4.5b). The median Arctic air mass surface pressure was on average 2.3 hPa higher in the warm season (April-October) but 1.2 hPa lower in the cold season (November-March), compared to the non-Arctic air masses. In both datasets, the surface pressure was higher in summer than in winter. The pressure variability was also larger in winter in both datasets, which can be explained by higher cyclonic activity due to enhanced meridional temperature gradient between the mid-latitudes and the polar regions.

Without creating average surface pressure composites for Arctic and non-Arctic conditions, it is hard to speculate the reason behind the differences in the observed air pressure between the datasets. Very low average surface pressure cannot be expected in Arctic conditions, if Arctic air is typically channelled to Värriö in the situation when a low pressure system is located several hundred kilometres north or north-east of Värriö, and is likely in a mature stage by then. The situation for the non-Arctic air masses may be different, as cyclones can approach from the south when they are potentially deeper than the ones over the Arctic ocean north of Värriö. However, noise in the pressure data is large, so further speculation is not done in this study.

Wind speeds measured at SMEAR I in Arctic and non-Arctic conditions were also briefly analysed (not shown). Wind speeds in both datasets were greater in winter than in summer, which is probably due to enhanced cyclonic activity in the cold season. The annual median wind speeds associated with the Arctic and the non-Arctic air masses were on average 3.4 m s^{-1} and 3.5 m s^{-1}, respectively.

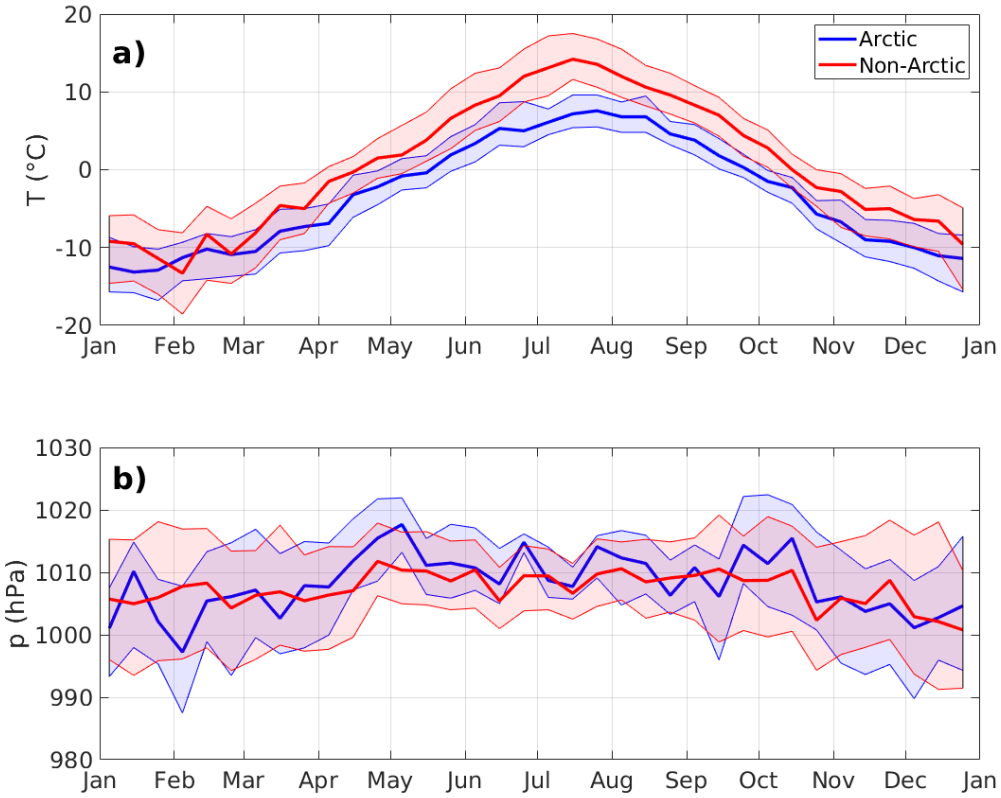

Figure 4.5: The median annual variation of a) temperature and b) atmospheric pressure reduced to sea level at SMEAR I in Värriö for the Arctic and the non-Arctic air masses in 1998-2017. The thick line is the median value and the shading indicates the area between the 25 and 75 % quartiles. An average over 10 days is applied to the data.

Humidity and global radiation

Relative humidity (RH) was found to be high in winter months between November and March in both Arctic (average 88.1 %) and non-Arctic (90.8 %) air masses (Figure 4.6a), which is typical for a maritime climate. In the beginning of March the air got drier, although the variability also increased drastically. The Arctic air masses did not clearly stand out from the non-Arctic air masses regarding RH. A small difference between the datasets was observed in spring, when the Arctic air masses were on average a little bit drier than the non-Arctic air masses.

In addition to relative humidity that depends on the temperature of the air, absolute humidity was also examined. Absolute humidity is the measure of water vapour in a volume of air (unit g m^{-3}) and is shown in Figure 4.6b. In months between April and October, the Arctic air masses had 1.8 g m^{-3} (27.2 %) lower moisture content than the non-Arctic air masses on average. The difference in median absolute humidities peaked

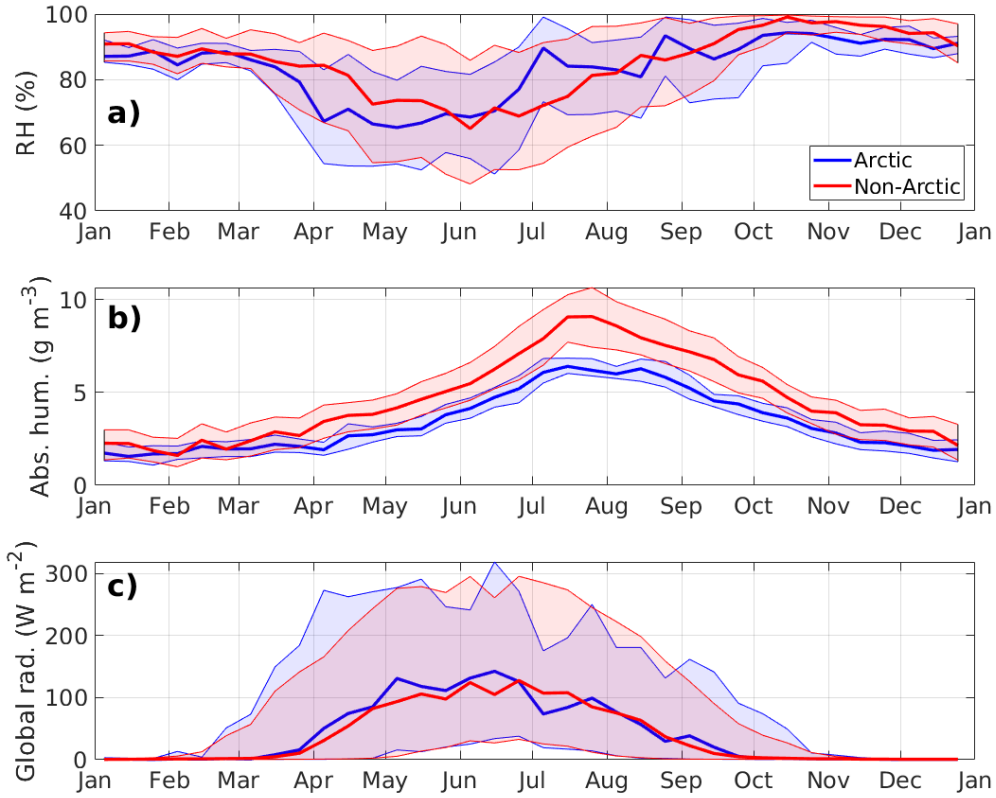

Figure 4.6: Median annual variation of a) relative humidity, b) absolute humidity and c) global radiation at SMEAR I in Värriö for Arctic and non-Arctic air masses in 1998-2017. The thick line is the median value and the shading indicates the area between the 25 and 75 % quartiles. An average over 10 days is applied to the data.

in July (2.9 g m^{-3}, 28.3 %). For those months, the 25 % quartile absolute humidity curve of the non-Arctic air masses was at or above the 75 % quartile of the Arctic air masses. This implies that absolute humidity is a good characteristic tracer of Arctic air masses in summer, but much less so in the cold season (November-March), when the difference between the Arctic and the non-Arctic air masses was only 0.6 g m^{-3} on average. However, the absolute humidity values in winter months are much smaller overall. The similarities in the annual variation of temperature (Figure 4.5a) and absolute humidity are apparent.

Global radiation can be used as a proxy for cloudiness, as a lower fraction of radiation can reach the ground in cloudy conditions. Global radiation observed at SMEAR I did not show large differences between Arctic and non-Arctic conditions (Figure 4.6c), which indirectly suggests that cloudiness is not notably altered by the air mass. During the median year, radiation was very limited in winter time, but started to increase rapidly in March. The median global radiation even in midsummer remained low, however, less than 150 W/m^2 on average. The overall variability in both datasets was large, which is largely

due to the diurnal cycle of incoming solar radiation. The Arctic data shows slightly larger variability in March and April. In July, when the difference in absolute humidity between the datasets was the largest (Figure 4.6b), the 75 % quartile was observed to be higher in the non-Arctic air masses.

Several effects could have caused the observed spring time dryness of the Arctic air masses relative to the non-Arctic air masses (Figures 4.6a, 4.6c). The non-Arctic air masses arriving from lower latitudes in April and May were likely affected by large surface moisture fluxes due to snowmelt. Additionally, as the meridional temperature gradient is still strong in spring months, the cold Arctic air masses are affected by large surface heat fluxes as they are transported to lower latitudes, which reduces relative humidity. Orographic processes may also play a role, especially if air parcels are transported via pathway 1 (Figure 4.3b).

In July, the higher relative humidity and lower global radiation in the Arctic air masses compared to the non-Arctic air masses could be due to the Arctic Ocean being at its warmest, which enhances the moisture flux to the atmosphere and makes the arriving Arctic air masses particularly maritime. The Arctic Ocean is, however, still colder than the surrounding regions, so that air mass might also get colder, which increases RH.

Overall, global radiation may not be a very representative variable to be used to analyse cloudiness. Incoming radiation also varies drastically seasonally and diurnally and for several months in winter it is very limited or non-existent.

Precipitation

The averaging method used for precipitation variables was the mean, and not the median, because the mean value is more representative of the total cumulative precipitation. The average year of precipitation intensity for precipitating hours is shown in Figure 4.7a and precipitation frequency in Figure 4.7b based on observations from the optical disdrometer. Precipitation frequency means the percentage of time precipitation occurs in an hour defined as Arctic or non-Arctic. The hours of no precipitation were excluded when the precipitation intensity was calculated. Noise in the data was quite large, probably due to limited data availability from the optical disdrometer (2008-2017, Figure 3.2).

Both in the Arctic and the non-Arctic air masses, precipitation intensity was the lowest in winter and the highest in summer, which is connected to the available moisture content (Figure 4.6b), as can be expected. In winter the Arctic air masses had similar precipitation intensity, but precipitated much less frequently than the non-Arctic air masses. In summer, Arctic air mass precipitation was lighter but the frequency of rain was higher than in the non-Arctic air masses. The high frequency of precipitation and therefore cloudy conditions related to the Arctic air masses might explain the observed lower

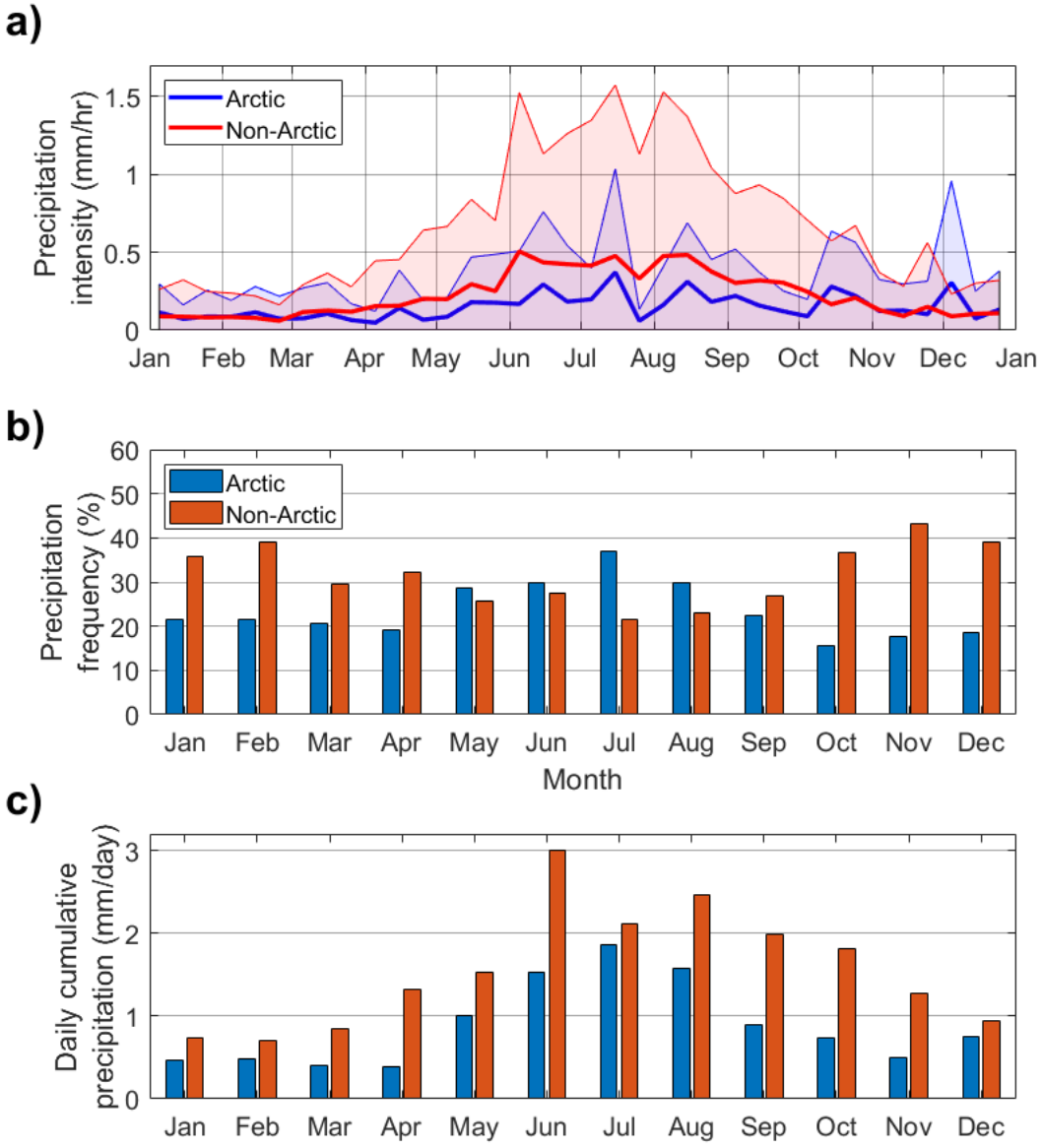

Figure 4.7: The mean a) precipitation intensity, b) precipitation frequency and c) the cumulative daily precipitation in 2008-2017 at SMEAR I, Värriö. Thick line represents the mean value (and not the median) and the shading indicates the area between the 25 and 75 % quartiles for the Arctic (blue) and the non-Arctic (red) air masses. Hours of no precipitation were excluded when precipitation intensity was calculated. Cumulative daily precipitation was calculated by multiplying the mean precipitation intensity with the precipitation frequency for each month and the number of hours in a day.

global radiation in July (Figure 4.6c), compared to the non-Arctic air masses, which had higher moisture content but precipitated with a higher intensity. The annual mean precipitation intensity was 0.15 mm h^{-1} and 0.23 mm h^{-1}, and the frequency of precipitation was 23.5 % and 31.7 % for the Arctic and the non-Arctic air masses, respectively.

Most precipitation from non-Arctic air masses is likely to be of frontal origin, which explains the lower precipitation frequency in summer than in winter, due to low cyclonic activity in the warm season. The precipitation frequency in the Arctic air masses was found to be the highest in summer, when the moisture content of the air is also notably higher (Figure 4.6b).

The daily cumulative precipitation (Figure 4.7c) describes the sum of precipitation during an average day of either Arctic or non-Arctic air mass. In all months the non-Arctic air masses precipitate more (mean annual precipitation 1.6 mm day^{-1}) than the Arctic air masses (0.9 mm day^{-1}). In winter months the difference is mostly explained by higher frequency of precipitation, whereas in summer the differences in precipitation intensity are more pronounced.

Comparing precipitation instruments

The optical precipitation instrument was chosen over the traditional tipping-bucket rain gauge because the use of the rain gauge is limited to liquid precipitation, even though longer timeseries would have been available for that instrument. Warm season (typically from May to October) cumulative rainfall data were compared between the two instruments (Figure 4.8a) for the Arctic and non-Arctic data combined. The comparison shows a close match between the instruments, although in 2011 the difference was more than 100 mm. A possible explanation for the larger difference in some of the years is the calibration needs of the optical instrument, as it is prone to bias if not operated properly (Moraes Frasson et al., 2011).

The number of hours associated with precipitation was also compared between the rain gauge and the optical disdrometer (Figure 4.8b). The sensitivity of the disdrometer to detect precipitation is much higher than that of the rain gauge (detection limits of 0.01 mm min^{-1} and 0.2 mm min^{-1}, respectively). This is why in Värriö the disdrometer records rainfall almost twice as often than the rain gauge in each of the years compared. These findings show that there is high probability of the rain gauge being unable to detect the lightest rainfall accurately. However, the cumulative rainfall measurements generally matched well, so this lightest rain that is not detected by the rain gauge probably does not contribute much to rainfall accumulation. The data from the optical disdrometer was used, because it can take observations of both liquid and solid precipitation, even though data for that instrument is available for 2008-2017 only.

Meteorological indices

Possible correlation between the Arctic air mass observation frequency and two meteorological indices, Northern Atlantic Oscillation (NAO)(Barnston and Livezey, 1987) and

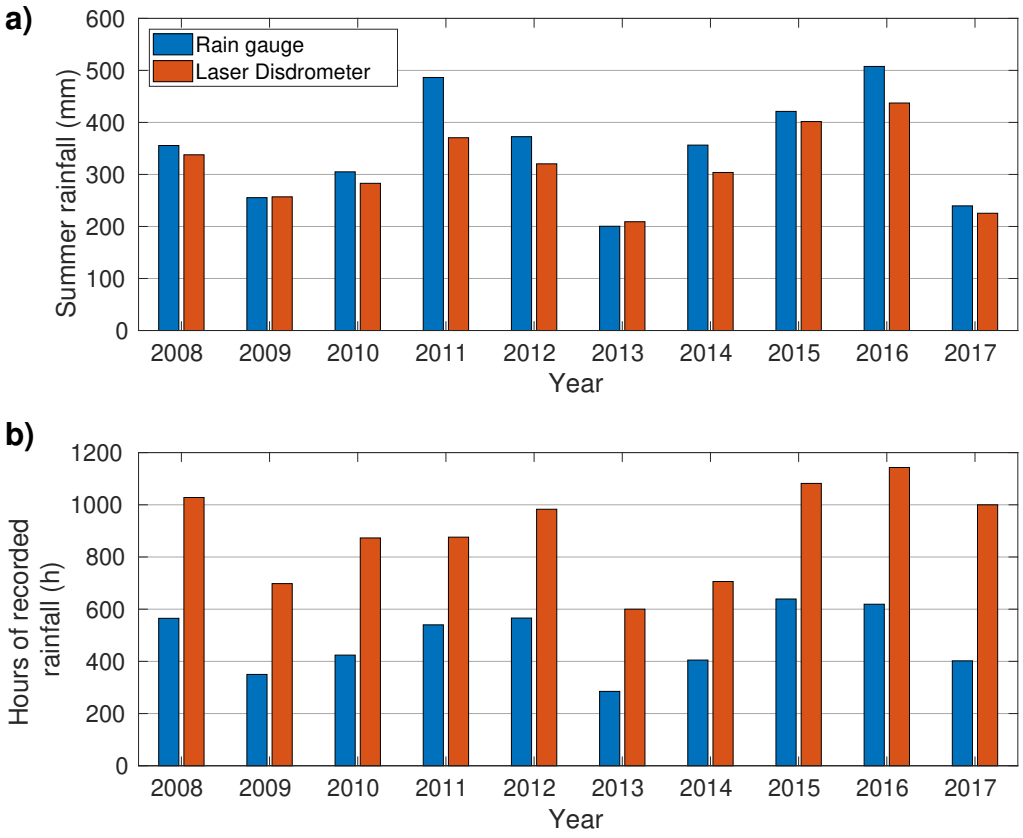

Figure 4.8: Comparison of a) liquid rainfall accumulation and b) the sum of precipitating hours using a traditional rain gauge (blue) and an optical disdrometer (red) for summer seasons in 2008-2017 at SMEAR I in Värriö. Comparison was made only for hours when both instruments were operational in the warm season (typically between May and October). In calculation of the sum of precipitating hours, an hour with any precipitation was counted as precipitating. Both Arctic and non-Arctic data were combined for the comparison.

Arctic Oscillation (AO)(Thompson and Wallace, 1998), were tested. To test the correlation, daily index data were downloaded from National Oceanic and Atmospheric Administration (NOAA) Climate Prediction Center (http://www.cpc.ncep.noaa.gov/). These daily index values were then compared to the number of hours that were associated with an Arctic air mass per day. Only days when the index in question was >1.0 or <-1.0 were included in correlation tests to have comparable results with a study by Trigo et al. (2002) who used monthly NAO values from 1958-1997 in their analysis.

Sample sizes for testing the correlation with NAO and AO were n=474 and n=972, respectively. A statistically significant, weak negative correlation between the daily NAO index and the daily number of hours associated with an Arctic air mass was found (R=-0.18, p=0.0001). No statistically significant correlation was found with the AO index (R=-0.05, p=0.135).

The statistically significant weak negative correlation with the daily NAO index found is in line with the findings by Trigo et al. (2002), who analysed 10 m wind anomalies associated with high (>1.0) and low (<-1.0) NAO index (Figures 3 and 4 in Trigo et al., 2002). A moderate northerly wind anomaly was found in the region from where the Arctic air masses arrive in Värriö (Figure 4.3) when NAO index was negative. The northerly flow anomaly did not appear to be clearly linked to either cyclonic or anticyclonic anomalies. The correlation found in this study is weak however, hence the NAO index remains a poor proxy to use for identification of Arctic conditions in Värriö and the AO index cannot be used as a proxy at all.

4.2.2 Aerosol Particles

Both the Arctic and the non-Arctic air masses arriving at SMEAR I had similar seasonal variation in the median particle size distribution (Figures 4.9a and 4.9c). In both cases there were clearly two modes, the Aitken and the accumulation mode. There was a notable difference in the number concentrations between the datasets; the mean total concentration during a median year was 308 cm^{-3} and 646 cm^{-3} in the Arctic and the non-Arctic air masses, respectively. Between November and March the average particle concentration was only 129 cm^{-3} in the Arctic air masses. The corresponding value for the non-Arctic air masses was 334 cm^{-3}. However, these are both very low values, as the particle concentration in urban air is typically thousands or tens of thousands per cm^3 (Bismarck-Osten et al., 2013).

The median value of CS had large seasonal variability in both of the datasets (Figures 4.9b and 4.9d). It ranged from 0.2 x 10^{-3} s^{-1} to 0.8 x 10^{-3} s^{-1} in the Arctic air masses and from 0.5 x 10^{-3} to 2.7 x 10^{-3} s^{-1} in the non-Arctic air masses. The value of CS in the non-Arctic air masses was on average 190 % larger than that of the Arctic air masses during the median year. This is caused by both lower number of total particles and modes being in smaller size ranges. The typically low value of CS in Arctic air masses means that the conditions are ideal for NPF, given that there are sources of nucleating and condensing vapours (Sogacheva et al., 2005).

Monthly median size distributions and the 25 % and 75 % quartiles are presented in Figure 4.10. The Aitken mode peak was in smaller sizes in the Arctic air masses, at the diameter range of approximately 25-40 nm depending on the season, whereas in the non-Arctic air masses the range was between 30 and 90 nm. The accumulation mode peak was at similar particle sizes in both datasets, at approximately 150-200 nm. The nucleation mode and the lower end of the Aitken mode were more pronounced in the Arctic air masses compared to the non-Arctic air masses in months between April and October. In particular, the 75 % quartile shows some signs of nucleation as elevated

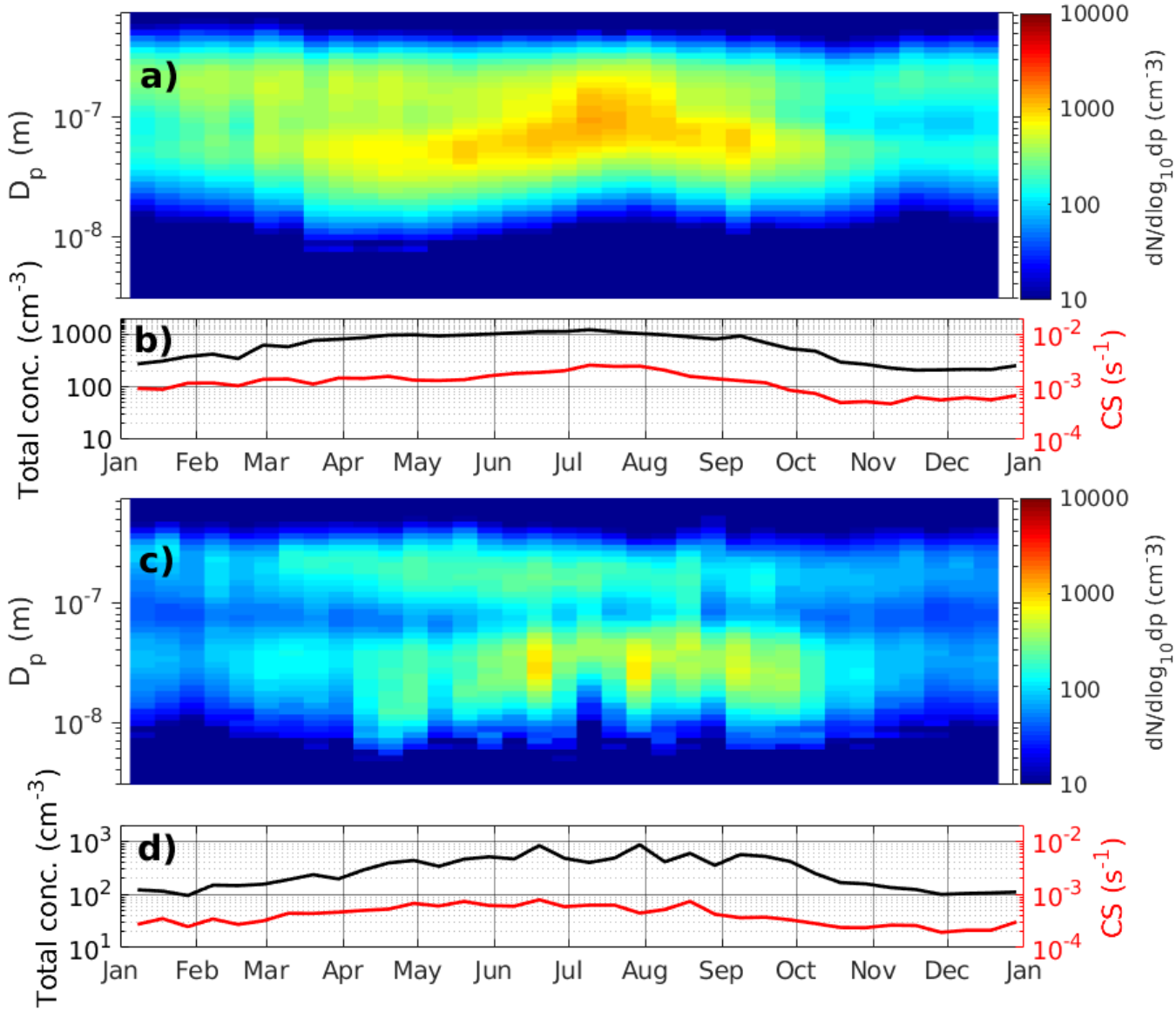

Figure 4.9: The median number size distribution, total concentration and condensation sink (CS) of aerosol particles at SMEAR I in 1998-2017 for the non-Arctic (a and b, respectively) and the Arctic (c and d, respectively) air masses. The data are from a differential mobility particle sizer (DMPS).

concentrations in spring and summer months. In other months the nucleation mode was practically non-existent in both datasets.

In the size distributions of both datasets, there was a clear concentration minimum between diameters 80 nm and 100 nm, approximately. The double-peaked size distribution of particles can be attributed to cloud processes and is a typical feature in maritime environments (Hoppel et al., 1986). When aerosol particles reach the critical diameter to activate as CCN, they grow further in size due to in-cloud scavenging processes and aquous phase oxidation of trace gases, namely SO_2. The subsequent evaporation of cloud

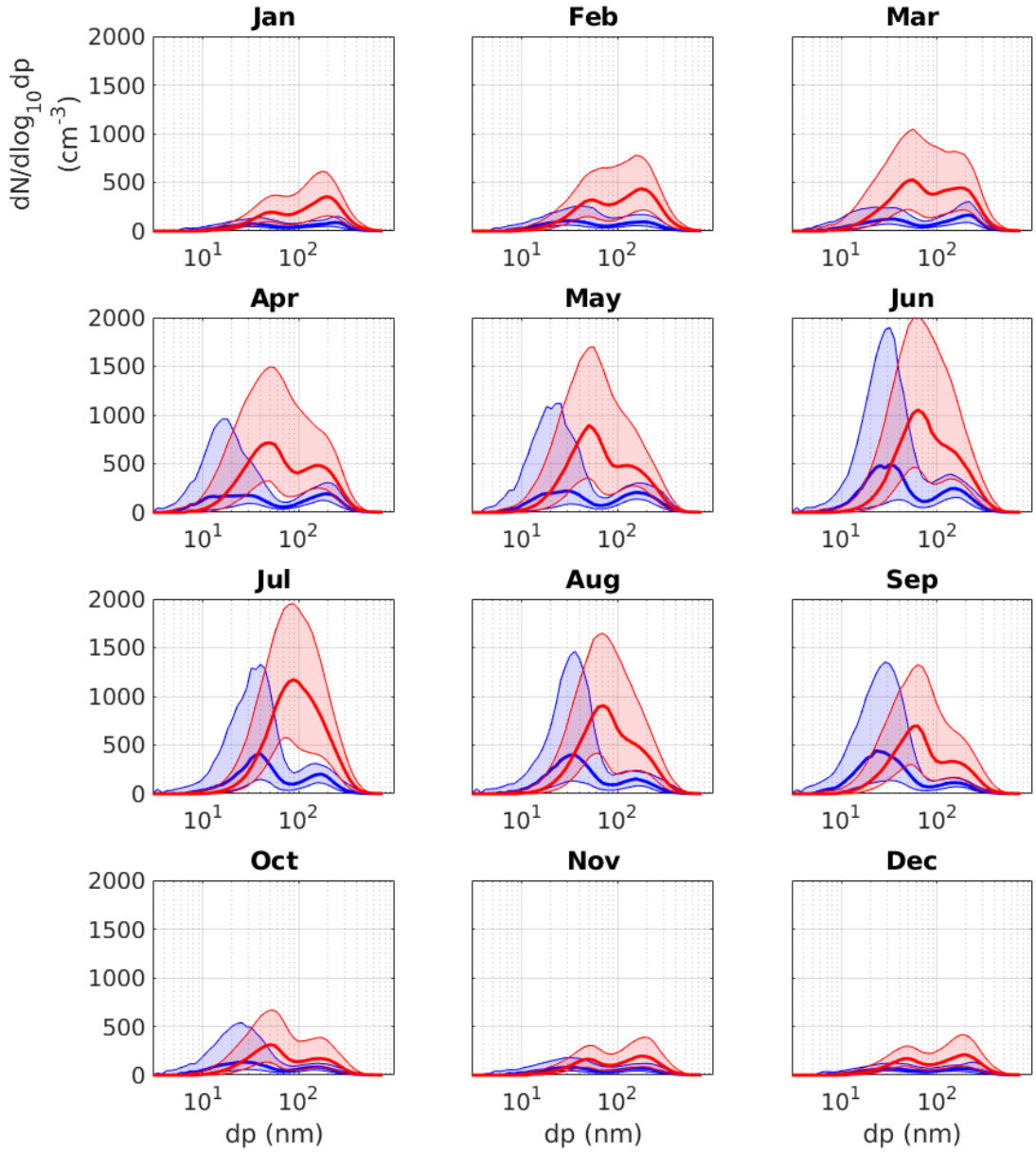

Figure 4.10: The median particle number size distribution for each month separately. Red represents the non-Arctic air masses, blue represents the air masses classified as Arctic. The thick line is the median value and shading marks the boundaries between the 25 % and 75 % quartiles. The horizontal axis is logarithmic.

droplets leaves behind notably larger particles than the critical size for activation. The modification of size distribution by non-precipitating clouds is an important process to take into account, as globally only one tenth of clouds reach precipitating stage (Pruppacher and Klett, 2012). The critical diameter for particles to activate as CCN in the region was found to be 70-80 nm for the Arctic air masses and 80-90 nm for the non-Arctic air masses, depending slightly on the season. This finding is in line with observations by Lihavainen et al. (2003) at the Pallas station, 225 km to the west of SMEAR I. They

found that nearly all particles that were larger than 80 nm in diameter were incorporated in cloud processes.

The size of the smallest particles observed in the median size distribution varied seasonally in both datasets as shown in Figures 4.9a and 4.9c. The size of the smallest particles was larger in winter and summer, and smaller in spring and autumn. The winter maximum might be explained by the extremely low nucleation rates due to the low concentration of biogenic VOCs (Hakola et al., 2012). The summer maximum is likely due to higher temperatures than in spring and autumn and therefore enhanced biogenic VOC emissions (Kourtchev et al., 2016), which leads to higher growth rates of ultrafine particles towards Aitken mode particles. The timing of this maximum in late July coincides well with the timing of maximum temperature observed (Figure 4.5a).

Comparison of observed aerosol size distributions with earlier studies

Asmi et al. (2011) analysed particle size distribution data from 24 field stations in Europe. The data were collected during a two-year period in 2008-2009. One of the stations, the Zeppelin Station (Ström et al., 2003), is located in Svalbard (78°58'N, 11°53'E), exactly in the region where most of the Arctic air masses that were studied here originated from. The seasonal variation in the particle size distribution at the station is shown in Figure 4.11.

There are similarities in the particle size distributions measured at SMEAR I and at the Zeppelin Station. Both stations observe the same modes in the same diameter ranges. In Värriö, the Aitken mode is dominant over the accumulation mode in spring, summer and autumn, while in winter both modes are weak. In Svalbard, the Aitken mode is dominant only in summer, when the resemblence in the size distributions of the two locations is particularly strong.

The most notable difference in the distributions can be seen in spring. At the Zeppelin Station the accumulation mode is clearly pronounced, which is not the case at SMEAR I. This might be due to primary aerosol particle emissions in spring, as sea ice retreats but the synoptic scale weather is still characterised by low pressure systems and high wind speeds. The particles of that mode are not observed in Värriö, so they are likely removed from the air by dry and wet deposition prior to arrival at SMEAR I.

4.2.3 Atmospheric Trace Gases

Sulphur dioxide (SO_2)

During the median year, SO_2 had a median concentration of 0.10 ppb in the non-Arctic dataset and 0.04 ppb in the Arctic dataset (Figure 4.12a). In the Arctic dataset the data

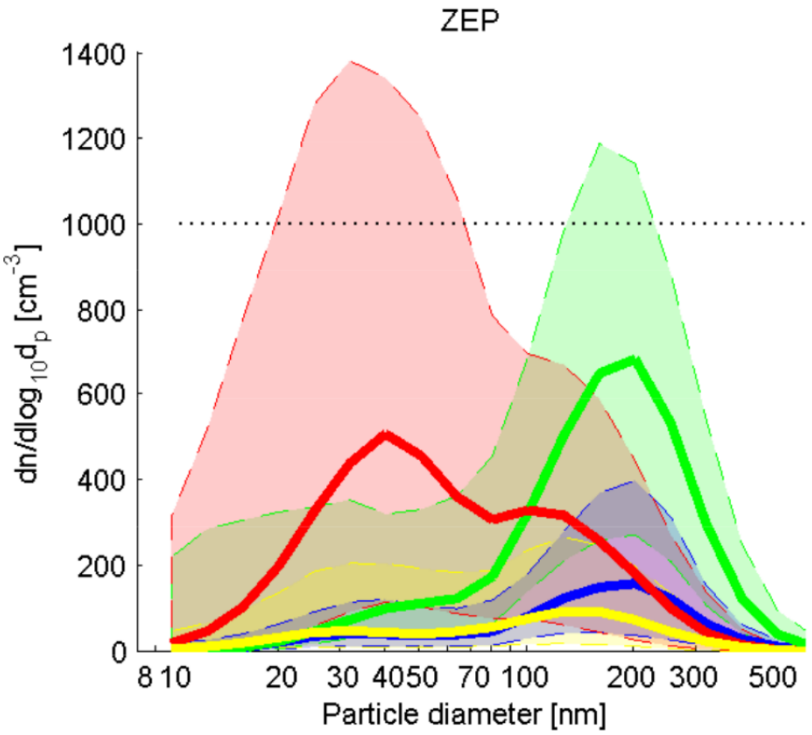

Figure 4.11: Statistical particle size distributions from Zeppelin Station, Svalbard during 2008-2009. Median distribution as solid line, 16th and 84th percentile distributions as shaded area. Green, red, yellow and blue denote the seasons: spring (MAM), summer (JJA), autumn (SON) and winter (DJF), respectively. (From Asmi et al., 2011)

was noisy especially for summer (from May to September) and winter (December and January). In the non-Arctic data there was no peaks in summer, but the winter peak was pronounced.

An important reason behind the winter peak is the seasonal cycle of the mixed layer height. In high-latitude winter, due to strong inversions, mixing is typically limited to a shallow layer, so the pollutants are diluted in a smaller layer. This phenomenon has a drastic effect on aerosol and trace gas concentrations especially in urban areas (Janhäll et al., 2006), but is likely experienced in Värriö as well. The relative importance of this effect is most notable for short-lived trace gases due to their usually low background concentration.

The winter peaks in the concentrations of SO_2 were not pronounced in the Arctic data set, probably because the Arctic air masses are much less affected by local and regional minor sources of pollution.

The high variability of summertime SO_2 concentration in the Arctic air masses could be due to an enhanced influence of the Kola Peninsula industry (Figure 4.3c) and, especially during the phytoplankton bloom season, due to the production of dimethyl sulphide (Park et al., 2017). The Kola Peninsula influence is further discussed in section 4.3.

Nitrogen oxides (NO_X)

The observed seasonal variation in the concentration of NO_X was similar to that of SO_2. The concentration was very low in Arctic air masses throughout the year(Figure 4.12b). In the non-Arctic air masses, the median concentration during the year peaked in February (0.61 ppb) and was only just above the detection limit of 0.1 ppb from May through September. In the Arctic dataset the annual cycle was similar but the median concentration was lower. The average concentration of NO_X during the median year was 0.10 ppb for the Arctic and 0.29 ppb for the non-Arctic air masses. As much as 46.4 % of the time the concentration of NO_X in Arctic air masses was below the detection limit of the instrument. The corresponding number for non-Arctic air masses was much lower, albeit still large (24.7 %).

In addition to the seasonal variation in the thickness of the mixed layer, the winter peak in the concentration of NO_X likely has a contribution of anthropogenic origin, too. Domestic heating related to the cold season likely causes notable emissions of both trace gases and aerosol particles (Tissari et al., 2008). The winter tourism season in Lapland is also at its peak from December to March (Vuoristo, 2002), which likely has an effect on local chemical composition via emissions from traffic and enhanced domestic heating.

Carbon monoxide (CO)

The seasonal variation in the median concentration of CO in both datasets resembles a sinusoidal shape (Figure 4.12c). In both datasets, the lowest annual median concentration was reached in July (85.8 and 99.6 ppb for the Arctic and the non-Arctic air masses, respectively), after which the concentration started to build up during autumn and winter. The highest concentration in the non-Arctic air masses was reached in February (177 ppb) and in March in the Arctic air masses (159 ppb). The concentration of CO decreased rapidly in spring. The annual median concentration of CO was 127.3 ppb for the Arctic and 135.9 ppb for the non-Arctic air masses. In general, the annual cycle of the CO concentration was very similar in both datasets, which suggests that CO is well mixed in the region and the effect of local sources of CO is weak.

Due to the long tropospheric residence time of CO, the regional background concentration dominates, which explains the similar concentrations in both datasets. The only clear sign of local anthropogenic sources in the concentration of CO was observed in non-Arctic air masses in January and February, when those air masses had on average 17.1 ppb higher concentration of CO than the Arctic air masses. This winter peak is likely due to enhanced local-scale emissions sources, as was discussed regarding NO_X. The Arctic air masses are much less affected by these sources.

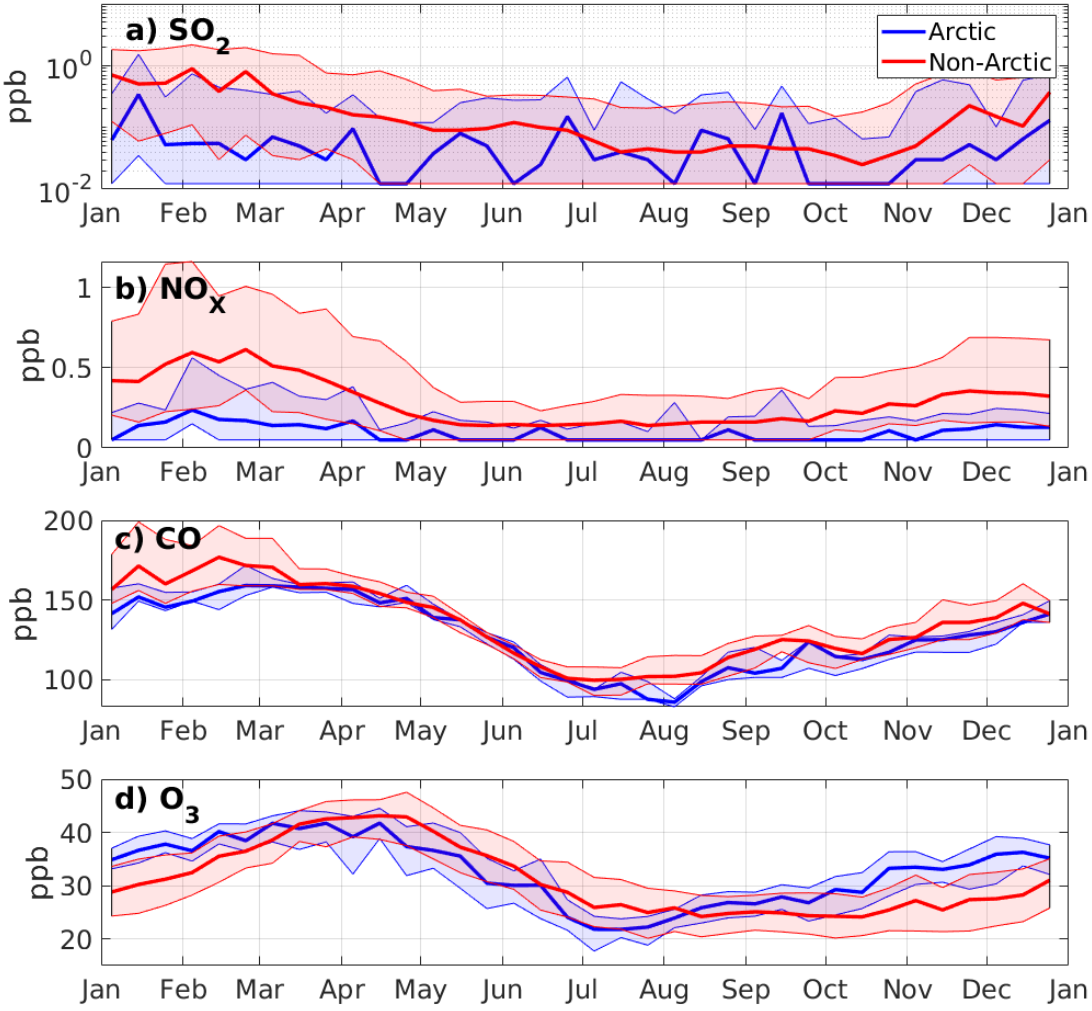

Figure 4.12: Median annual concentration variation of a) sulphur dioxide (SO_2), b) nitrogen oxides (NO_X), c) carbon monoxide (CO) and d) ozone (O_3) at SMEAR I in Värriö in 1998-2017 (for CO 2008-2017), for Arctic and non-Arctic air masses. The thick line is the median value and the shading indicates the area between the 25 and 75 % quartiles. An average over 10 days is applied to the data. The y-axis is logarithmic in subfigure a.

In spring, the oxidation of CO (and the production of ozone) begins, reducing the concentration of CO in both Arctic and non-Arctic air masses. The spring time maximum and late summer minimum are typical features of concentrations of both CO and ozone in mid- and high-latitude locations in the northern hemisphere (Parrish et al., 1998).

Ozone (O_3)

Similar to the concentration of CO, the seasonal variation of the median concentration of ozone is approximately sinusoidal. Owing to the relatively long tropospheric residence time, the background concentration of ozone in Värriö is important, albeit the variation between the datasets is larger than it was for CO, which implies that ozone is not as well mixed throughout the hemisphere.

The concentration of ozone also peaked in late winter or early spring in both the Arctic and non-Arctic datasets (peak median values of 41.8 ppb and 43.1 ppb, respectively), as shown in Figure 4.12d. The minimum median monthly concentration in the Arctic dataset was 21.8 ppb and 24.1 ppb for the non-Arctic air masses. The Arctic air mass median concentration of ozone in winter (October-February) was on average 4.6 ppb higher compared to the non-Arctic air masses. Unlike SO_2, NO_X and CO, the average annual concentration of O_3 was higher in the Arctic air masses (33.7 ppb) than in the non-Arctic air masses (31.0 ppb). The difference was particularly clear in months between November and February, when the concentration of O_3 was on average 24.6 % higher in Arctic air masses (35.9 ppb) compared to the non-Arctic air masses (28.8 ppb). The observed annual range of variation in the median concentration of ozone is in line with Vingarzan (2004), who found that the annual variation in the northern hemisphere is within 20 ppb and 45 ppb, depending on the location.

It has been proposed already several decades ago, that the winter peak of ozone is due to enhanced stratospheric transport of ozone to the mixed layer in that season (Oltmans, 1981). However, Dibb et al. (2003) showed that it only accounts for about 85 % of the background concentration of ozone, but not the peak itself. Vingarzan (2004) concluded that the peak is the result of increase in solar radiation acting upon the pool of NO_X that has accumulated during the dark season. As CO is also a precursor of ozone, the concentration of CO begins to decrease as soon as more radiation becomes available. These processes explain why the peak of ozone is some weeks later than its precursors.

The higher average concentration of ozone in the Arctic air masses compared to the non-Arctic air masses in winter is likely linked to suppressed sinks in the Arctic. In cold environments, dry deposition on ice and sea surfaces is weak and wet deposition on the other hand is weak because of the extremely low moisture content, which increases the tropospheric residence time of ozone (AMAP, 2015). However, in summer the concentration of ozone was observed to be higher in the non-Arctic air masses. This finding may be related to increased concentration of biogenic VOCs from the continent to the non-Arctic air masses, as they act as a precursor of ozone.

4.3 The Kola Peninsula Influence

The Kola Peninsula industrial sites, namely Nikel and Monchegorsk (Figure 3.1), are not only the largest atmospheric SO_2 source in the Scandinavian region, but some of the most emitting point sources globally (Benkovitz et al., 1996). Even though socio-economic regulation in Russia has successfully decreased the emissions from the non-ferrous metal smelters of the Kola Peninsula, the region remains the largest pollution source affecting observed air quality at SMEAR I (Kyrö et al., 2014). It is hence justified to study the impact of the Kola Peninsula industry on atmospheric composition of Arctic air masses.

The number of hours an air mass spent within 50 km of the Kola Peninsula industrial sites while in the mixed layer was calculated for each trajectory. Of all the trajectories that originated from the Arctic, 80.3 % were not transported through these industrial sites (Figure 4.13). The trajectories that were, spent on average 3.8 hours in the vicinity of either of the sites. Less than one percent of the trajectories associated with an Arctic air mass spent more than 6 hours near the industrial sites, which greatly increases the risk of noisy data. Thus, those cases were excluded from the analysis of the effect of Kola Peninsula influence on aerosol particle and trace gas concentrations.

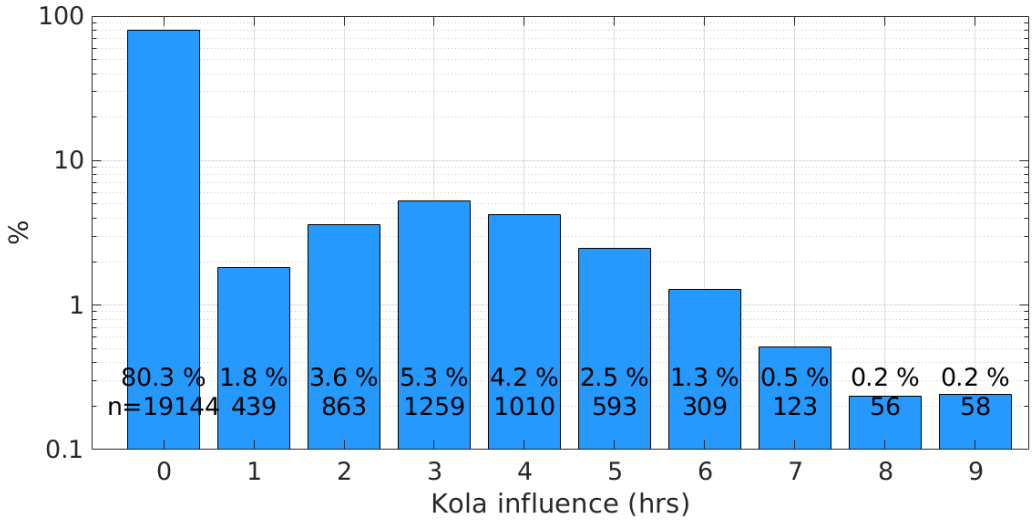

Figure 4.13: The number of hours an air parcel spent within 50 km of either Nikel or Monchegorsk industrial sites while in the mixed layer was counted for trajectories associated with an Arctic air mass that arrived at SMEAR I in 1998-2017. The number of trajectories in each class and the corresponding percentage of the total number of trajectories, is shown. The analysis is based on HYSPLIT model backward trajectories.

The concentrations of nucleation, Aitken and accumulation mode particles steadily increased with increased Kola Peninsula influence (Figure 4.14). The median concentration of the Aitken mode particles increased most notably, from 46 cm^{-3} in unaffected Arctic air masses to 131 cm^{-3} when the air mass spent 6 hours in the vicinity of the

sites (185 % increase). The corresponding increase in the concentration of nucleation and accumulation modes were from 35 cm^{-3} to 71 cm^{-3} (103 % increase) and 50 cm^{-3} to 105 cm^{-3} (110 % increase), respectively. The increase in both nucleation and accumulation mode particles implies that both primary NPF enhancement and primary aerosol emissions had a contribution to the total particle concentration increase. The median total particle concentration increased from 170 cm^{-3} to 388 cm^{-3} (128 % increase), but the percentage increase in CS was even greater, from 0.34 x 10^{-3} s^{-1} to 1.04 x 10^{-3} s^{-1} (206 %), when the Kola Peninsula influence increased to 6 hours compared to unaffected air masses. Large increase in CS is likely to hinder NPF, as large values of CS decrease the lifetime of potentially nucleating vapours.

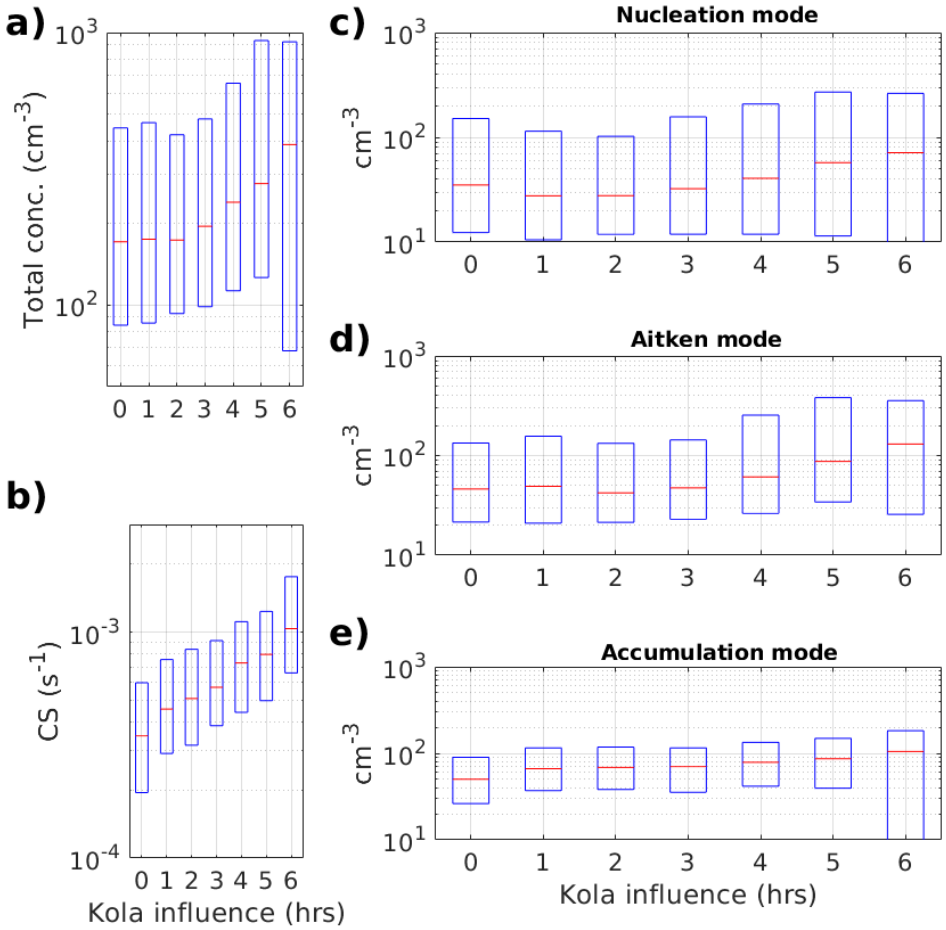

Figure 4.14: The effect of the Kola Peninsula industrial sites on a) total aerosol particle concentration, b) condensation sink (CS), c) nucleation (3-25 nm), d) Aitken (25-90 nm) and e) accumulation (90-1000 nm) mode particles. The red lines indicate median values and the 25 and 75 % quartiles are marked with the blue boxes. The data is from SMEAR I in Värriö from 1998-2017 and the analysis is based on HYSPLIT backward trajectories.

The changes in the concentrations of SO_2, NO_X, CO and O_3 as a function of the Kola Peninsula influence are shown in Figure 4.15. The concentration of SO_2 steadily increased from 0.03 ppb median value at 0 hours of influence to 0.58 ppb at 6 hours, which corresponds to a 18-fold increase. There was no notable change in the concentration of NO_X. When NO_X were analysed separately for NO and NO_2 (by extracting concentration of NO from that of NO_X), there was no observed variation in the concentration of NO above the detection limit. The measured concentrations of NO_X are so close to the detection limit (0.1 ppb), that analysing patterns from the data might not be a feasible thing to do.

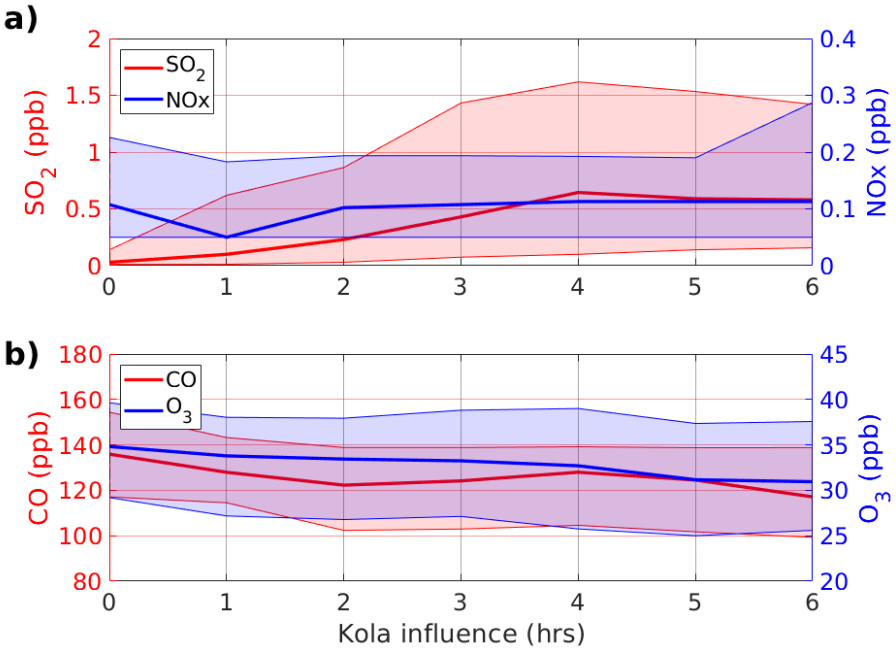

Figure 4.15: The effect of the Kola Peninsula industrial sites on trace gas concentrations of an air parcel for a) SO_2 and NO_X, and b) CO and O_3. The thick line represents the median concentration and the shading indicates the area between the 25 % and 75 % quartiles. The data are from SMEAR I in Värriö from 1998-2017 (2010-2017 for CO).

The variations in the concentrations of CO and O_3 caused by the influence of the Kola Peninsula industry were also analysed (Figure 4.15b). A steady decrease in the concentration of both gases was observed as the Kola Peninsula influence duration increased. This is a somewhat surprising finding, as it would be expected that at least the concentration of CO would increase due to anthropogenic emissions. One possible explanation is that in summer months (JJA) pathway 2b is overrepresented compared to other seasons (Figure 4.3c). Because the non-affected air masses are mostly from other than summer months (Figure 4.1), the observed decreasing trend might be connected to the seasonal cycle of these gases instead of the Kola Peninsula influence. Thus, this analysis would be best done separately for different seasons.

4.4 Sources of Uncertainty

Used method

Some sources of uncertainty are associated with the method used. Arctic air masses were defined as those that have been poleward of 78° N or higher 72 hours before arrival. Using a constant latitude as a threshold is completely arbitrary and might not be an accurate description of reality. The boundary between Arctic and polar air masses is constantly changing in shape and varies meridionally as seasons change (Figure 2.2a). Not all Arctic air mass occurrences are captured by this method and on the other hand, some non-Arctic cases might be included.

The low frequency of Arctic air mass occurrences in summer months, especially in July, increases the uncertainty of the results for this season. Interpretation of results needs to be done with care for months with less data. In plots with 10-day averaging periods, each period in July consists of only about 320 data points in the Arctic dataset. However, with the use of median as the averaging method, individual data points with large deviation are smoothed out.

Trajectories (HYSPLIT)

Another clear source of uncertainty is the spatial and temporal resolutions of the gridded meteorological datasets used as input to run the trajectory model. Especially the FNL dataset that was used had a particularly coarse resolution (191 km, 6 hours). However, resolution is not the only thing that should be considered. For example, in the 0.5 degree dataset of GDAS, vertical motion component is not included and has to be explicitly calculated from horizontal divergence. This leads to errors larger than the benefits of the improved spatial resolution (Su et al., 2015). Linear temporal interpolation for time steps that fall between two output files of the meteorological dataset is likely to cause some uncertainty, especially as the region is characterised by a frequent occurrence of low pressure systems that have relatively short lifetimes.

The trajectory analysis shows that most air particles spent most of their time in the mixed layer prior to their arrival at SMEAR I. The boundary layer is not a simple part of the troposphere to model due to its turbulent nature. Surface roughness is an important factor in mechanical turbulence generation, especially at higher latitudes and in maritime environments where thermal turbulence generation is weak. Trajectory models do attempt to parametrise boundary layer dynamics, but some degree of uncertainty is likely caused by this. Attribution of observed elevated gas and particle concentrations to point like sources such as the Kola Peninsula industrial sites, however, needs to be considered with uncertainty when using a trajectory model. This is why a 50-kilometre

radius was considered with these point like sources, albeit some trajectories that are unaffected will be included in the analysis of affected air masses.

Initially a small error in a trajectory calculation grows rapidly as the length of the trajectory is increased. Decreasing the model run length to, for example, 48 hours with a lower latitude threshold would decrease the spatial error in determining the source region of the air parcel. However, at the same time the possibility of false air mass identification is increased, because the latitude threshold would need to be lower.

SMEAR I observations

Local emission sources could systematically bias the observations, if present. The location of the station has been intentionally chosen to represent pristine boreal forest conditions to avoid this problem. The station is near the Russian border and no roads or significant settlements exist in that part of Finnish Lapland. The population density remains very low towards the Arctic Ocean, which makes it unlikely that significant anthropogenic air mass modification takes place with the exception of the discussed Kola Peninsula industrial sites.

The concentrations of SO_2 and NO_X are frequently near or below the detection limit of the instruments measuring them. This may limit quantitative analyses of these gases, but differences between the two datasets are clear nonetheless. Background concentrations of the gases are naturally very low, but the seasonal variation of the median value or the 75 % quartile can be analysed from the data.

Time series of monthly averages for all variables analysed are presented in Appendix A to illustrate the inter-annual variability, which was observed to be large. This means that it is not possible to set any threshold values of meteorological variables or aerosol particle and trace gas concentrations to identify Arctic air mass events. On the other hand the measurement techniques have likely improved in 20 years, which means that the first years of measurements of SO_2 and NO_X should be used with care, as some signs of measurement bias were observed (Appendix A). The variety of measured variables at SMEAR I has also improved since 1998. For example, in late 2017 a Particle Size Magnifier (PSM, Vanhanen et al., 2011) was installed at SMEAR I to allow analysis of particles down to 1.5 nm in diameter.

4.5 Future Work

The used method of air mass identification is assumed to be valid for the purpose of this study due to long time series of observations available. For a case study, a more sophisticated trajectory model and higher resolution meteorological input data should be

used. For case studies, ensemble trajectory modelling can be helpful in assessment of errors in individual cases.

Further separation of the Arctic air mass dataset to the three observed main pathways for arriving air masses (pathways 1, 2a and 2b) could provide information on the influence of local sources along the pathway or if topography plays a role in changing the air mass properties. Open data available from the Zeppelin Station could be used to determine how air masses change in 72 hours as they are transported from Svalbard to Värriö, by comparing the same air masses. A similar study was done by Väänänen et al., 2013, who investigated the effect of time spent over the boreal forest on the NPF event probability. For this type of study, it would be ideal to use HYSPLIT with a higher temporal and spatial resolution gridded meteorological data set or perhaps a more sophisticated trajectory model. The influence of the Kola Peninsula could also be excluded to analyse only Arctic air masses that are least influenced by human activities.

One way to expand our understanding of the synoptic scale weather conditions associated with Arctic air mass occurrences would be to create composite surface pressure charts of average conditions at the time of arrival and, for example 24, 48 and 72 hours prior to the arrival, at SMEAR I. This could be done separately for pathways 1, 2a and 2b to examine if the northerly flow observed is connected to cyclonic activity.

Attention has recently been paid to anthropogenic particle and trace gas emissions due to air quality issues. It would hence be intriguing to study long-term annual trends of air mass properties of both Arctic and non-Arctic air masses. In non-Arctic air masses, particle and trace gas concentrations (especially SO_2) from anthropogenic sources have likely decreased due to emission regulations. On the other hand, the sea ice extent of the Arctic Ocean has steadily decreased in the recent decades, which exposes the overlying air masses to emissions of primary particles and secondary particle precursors. The reduction in sea ice extent would likely also increase the moisture and heat fluxes from the ocean surface to the atmosphere. Moreover, as climate change is estimated to have a pronounced warming effect on the Arctic region, temperature trends of Arctic air masses could be studied using the method that was employed here.

More in-depth statistical analysis could be performed to determine if Arctic and non-Arctic air masses differ in a statistically significant way. This should probably be done separately for winter and summer season at least, as the conditions seem to be quite different in many ways, the biggest difference between the seasons being the dramatic change in the incoming solar radiation. The average air temperature is above zero approximately from mid-April to mid-October (Figure 4.5a), which could be used as the study period for the summer season. Statistical significance could also be tested for different years separately for at least ozone to determine if it can reliably be used as a proxy for Arctic air masses in the winter season or not.

5. Summary and Conclusions

Long-term measurements at SMEAR I and a trajectory model were used to characterise Arctic air masses arriving in Värriö in 1998-2017. The main aim of this thesis was to examine what unique meteorological and atmospheric composition related properties Arctic air masses have as they arrive at the Eurasian continent. In particular, aerosol particle and trace gas concentrations of Arctic and non-Arctic air masses were compared. An additional aim was to study the conditions leading to Arctic events in Värriö and the relevance of trajectory path to the air mass properties.

In this study, an air mass was defined to be Arctic, if the latitude of an air parcel was poleward of 78° N 72 hours before arrival at SMEAR I based on the HYSPLIT model. Using this method, 15.0 % of all air masses were classified as Arctic. The seasonal variation was large; on average, Arctic air mass occurrences in March totalled 7.5 days, while the corresponding number for July was only 2.0 days.

The typical trajectory paths were found to be cyclonically curved, originating both from the east and west of Svalbard, which suggests that Arctic air mass events are connected to passing low pressure systems north-east and east of Värriö. This finding is supported by the short duration of individual events, as the median duration was 10 hours. Trajectory data also revealed that air parcels arriving at SMEAR I spend majority of the time in the mixed layer during the 72 hours prior to arrival in Värriö. In the warm season (May through October), 88.0 % of the trajectories spent at least 48 hours out of 72 hours in the mixed layer, whereas in the cold season (November through April) the corresponding fraction was 69.1 %. This difference was found to be due to the seasonal variation in the height of the mixed layer, as the average altitude of the air parcel along the path only had minor seasonal changes.

In the traditional air mass classification scheme (Bergeron, 1930), Arctic air masses are classified as colder and typically drier than other air masses. Based on observations in Värriö, Arctic air masses stand out as colder and have lower absolute humidity than non-Arctic air masses in most months, especially from June through August (5.6 °C average temperature difference). The temperature and moisture content differences between the datasets were much less pronounced in the cold season. The differences in the relative humidity between the datasets were minor. These findings suggest that the traditional air mass classification based on temperature and humidity can be useful in summer, but

is poor in winter due to the open Arctic Ocean and the related moisture and heat fluxes to Arctic air masses.

Precipitation frequency of the Arctic air masses was slightly higher than that of the non-Arctic air masses in summer, but in winter the opposite was observed. Rain rate was lower in the Arctic dataset compared to the non-Arctic dataset in all seasons. Air pressure associated with an Arctic air mass event was on average 2.3 hPa higher in months between April and October compared to non-Arctic air masses. A slight opposite anomaly was observed from April to October, when Arctic air masses had on average 1.2 hPa lower air pressure, although the noise in the pressure data was large. A weak correlation between daily NAO index (when the index was >1.0 or <-1.0) and the daily number of hours associated with an Arctic air mass was found to be statistically significant (R=-0.18, p=0.0001). The correlation with daily AO index was not statistically significant.

The median particle number size distributions observed in the Arctic and the non-Arctic air masses had similar features. The Aitken and accumulation modes were present in all the seasons, although their concentrations had a strong seasonal variation. The two modes were at slightly smaller diameter ranges in the Arctic air masses. The nucleation mode concentration was observed to be higher in the Arctic air masses in spring and summer months than in the non-Arctic air masses. In winter months, the nucleation mode was not present in either of the datasets. In both Arctic and non-Arctic air masses, a concentration minimum between the Aitken and Accumulation modes was observed due to cloud processing (Hoppel et al., 1986). The lower size limit of this minimum marks the critical diameter, when particles activate as CCN, and it was found to be approximately 80 nm in both datasets, depending slightly on the season.

The average total aerosol particle concentration of an Arctic air mass was 308 cm^{-3} during a median year and 129 cm^{-3} for months between November and March. The corresponding values for the non-Arctic air masses were 646 cm^{-3} and 334 cm^{-3}, respectively. Similarly the value of CS in Arctic air masses varied from 0.2 x 10^{-3} s^{-1} to 0.8 x 10^{-3} s^{-1}, and was on average 65 % smaller than in the non-Arctic air masses. The low value of CS makes Arctic air masses good bases for NPF events (Sogacheva et al., 2005).

The obtained monthly median particle size distributions measured at SMEAR I were compared with a similar study conducted in Svalbard, at the Zeppelin Station (Asmi et al., 2011). At both locations the size ranges of the peaks were similar, although there were more accumulation mode particles measured at the Zeppelin station, likely due to removal from air by deposition before arrival at SMEAR I.

Concentrations of SO_2 and NO_X were, on average, very low in Värriö, which is typical for a remote location. A similar seasonal variation pattern was observed in both datasets, albeit Arctic air masses had even lower average concentrations of those trace gases. The lowest concentrations were observed in summer and the highest in January

and February for both gases and both datasets. The likely explanation for the winter peak is the combined effect of lower mixed layer depth due to surface inversion and enhanced local sources due to domestic heating and the active tourist season in Lapland. In nearly half (46.4 %) of the hours associated with an Arctic air mass, the concentration of NO_X was below the detection limit.

The observed winter peaks in the concentrations of CO and O_3 during the median year were slightly later, in March and April, respectively. When solar radiation becomes available again in spring, O_3 production from its precursors begins, effectively reducing the concentration of especially CO. The minimum concentrations of both gases in both datasets were observed in July during the median year. The Arctic air masses were found to have on average 24.6 % higher concentration of O_3 in months between November and February compared to the non-Arctic air masses, making ozone a prominent tracer of Arctic air masses in the winter season. The variability in the concentration of CO was similar in the Arctic and the non-Arctic datasets, ranging from 85.8 ppb to 159 ppb and from 99.6 ppb to 177 ppb, respectively. The annual median concentration of CO was 127.3 ppb for the Arctic and 135.9 ppb for the non-Arctic air masses.

The two major industrial sites in the Kola Peninsula, located within 200 km from Värriö, were found to notably modify air masses arriving at SMEAR I. The concentrations of especially SO_2 and aerosol particles are affected if an air mass crosses an area of heavy industry. Both primary particle and secondary particle precursor emissions are the likely cause for the increased particle concentration in air masses affected by the Kola Peninsula industry. 19.7 % of the Arctic air masses were transported along a route that passes within 50 km of the two major Kola Peninsula industrial sites.

Several sources of uncertainty were discussed. Most notable sources of uncertainty derive from the used trajectory model and the coarse resolution gridded meteorological input data used to run it. Additionally, the used method to identify Arctic air masses based on constant latitude threshold is arbitrary and a seasonally varying threshold might be a better option. Some uncertainty also originates from the measurements, especially regarding the very low concentration trace gases of SO_2 and NO_X, which are frequently measured to be below the detection limit of the instruments.

To conclude, trajectory-based methods can be useful in identifying air masses. Individual Arctic air mass events in Värriö were found to be likely linked to low pressure systems in the Arctic Ocean. The traditional air mass classification based on temperature and humidity to identify Arctic air masses was found to be viable in summer, but not in other seasons. In winter, aerosol particle and trace gas (namely ozone) concentrations were found to be better alternative variables to be used to characterise Arctic air masses. However, transport over human-habited continent can have a major effect on the aerosol and trace gas properties of the air mass, even if the air mass originates from the Arctic.

Bibliography

Aalto, P. (2017). *Värriö Instruments*. URL: https://wiki.helsinki.fi/pages/viewpage.action?pageId=243959942 (visited on 03/18/2019).

Aalto, P., K. Hämeri, E. Becker, R. Weber, J. Salm, J. M. Mäkelä, C. Hoell, C. D. O'dowd, H.-C. Hansson, M. Väkevä, et al. (2001). "Physical characterization of aerosol particles during nucleation events". In: *Tellus B: Chemical and Physical Meteorology* 53.4, pp. 344–358.

ACIA (2004). "Impacts of a Warming Arctic". In: *Impacts of a Warming Arctic-Arctic Climate Impact Assessment*, p. 144.

AMAP (2015). "Black carbon and ozone as Arctic climate forcers". In: *Arctic Monitoring and Assessment Programme (AMAP), Oslo, Norway*, p. 116.

Arakaki, T. and B. C. Faust (1998). "Sources, sinks, and mechanisms of hydroxyl radical (OH) photoproduction and consumption in authentic acidic continental cloud waters from Whiteface Mountain, New York: The role of the Fe (r)(r= II, III) photochemical cycle". In: *Journal of Geophysical Research: Atmospheres* 103.D3, pp. 3487–3504.

Asmi, A., A. Wiedensohler, P. Laj, A.-M. Fjaeraa, K. Sellegri, W. Birmili, E. Weingartner, U. Baltensperger, V. Zdimal, N. Zikova, et al. (2011). "Number size distributions and seasonality of submicron particles in Europe 2008–2009". In: *Atmospheric Chemistry and Physics* 11.11, pp. 5505–5538.

Barnston, A. G. and R. E. Livezey (1987). "Classification, seasonality and persistence of low-frequency atmospheric circulation patterns". In: *Monthly weather review* 115.6, pp. 1083–1126.

Barrie, L. and R. Hoff (1984). "The oxidation rate and residence time of sulphur dioxide in the Arctic atmosphere". In: *Atmospheric Environment (1967)* 18.12, pp. 2711–2722.

Benkovitz, C. M., M. T. Scholtz, J. Pacyna, L. Tarrasón, J. Dignon, E. C. Voldner, P. A. Spiro, J. A. Logan, and T. Graedel (1996). "Global gridded inventories of anthropogenic emissions of sulfur and nitrogen". In: *Journal of Geophysical Research: Atmospheres* 101.D22, pp. 29239–29253.

Bergeron, T. (1930). "Richtlinien einer dynamischen Klimatologie". In: *Meteorologische Zeitschrift* 47.7, pp. 246–262.

Bismarck-Osten, C. von, W. Birmili, M. Ketzel, A. Massling, T. Petäjä, and S. Weber (2013). "Characterization of parameters influencing the spatio-temporal variability of urban particle number size distributions in four European cities". In: *Atmospheric environment* 77, pp. 415–429.

Carslaw, K., L. Lee, C. Reddington, K. Pringle, A. Rap, P. Forster, G. Mann, D. Spracklen, M. Woodhouse, L. Regayre, et al. (2013). "Large contribution of natural aerosols to uncertainty in indirect forcing". In: *Nature* 503.7474, p. 67.

Curry, J. (1983). "On the formation of continental polar air". In: *Journal of the Atmospheric Sciences* 40.9, pp. 2278–2292.

Dibb, J. E., R. W. Talbot, E. Scheuer, G. Seid, L. DeBell, B. Lefer, and B. Ridley (2003). "Stratospheric influence on the northern North American free troposphere during TOPSE: 7Be as a stratospheric tracer". In: *Journal of Geophysical Research: Atmospheres* 108.D4.

Draxler, R. and G. Hess (1997). "Description of the HYSPLIT4 modeling system. NOAA Tech. Memo. ERL ARL-224". In: *Natl. Oceanic and Atmos. Admin.* Vol. 24.

Habib, E., W. F. Krajewski, and A. Kruger (2001). "Sampling errors of tipping-bucket rain gauge measurements". In: *Journal of Hydrologic Engineering* 6.2, pp. 159–166.

Hakola, H., H. Hellén, M. Hemmilä, J. Rinne, and M. Kulmala (2012). "In situ measurements of volatile organic compounds in a boreal forest". In: *Atmospheric Chemistry and Physics* 12.23, pp. 11665–11678.

Hari, P., T. Petäjä, J. Bäck, V.-M. Kerminen, H. K. Lappalainen, T. Vihma, T. Laurila, Y. Viisanen, T. Vesala, and M. Kulmala (2016). "Conceptual design of a measurement network of the global change". In: *Atmospheric Chemistry and Physics* 16.2, pp. 1017–1028.

Hari, P. and M. Kulmala (2005). "Station for Measuring Ecosystem-Atmosphere Relations (SMEAR II)". In: *Boreal Environment Research* 10, pp. 315–322.

Hari, P., M. Kulmala, T. Pohja, T. Lahti, E. Siivola, L. Palva, P. Aalto, K. Hämeri, T. Vesala, S. Luoma, et al. (1994). "Air pollution in eastern Lapland: challenge for an environmental measurement station." In: *Silva Fennica* 28.1.

Hoppel, W., G. Frick, and R. Larson (1986). "Effect of nonprecipitating clouds on the aerosol size distribution in the marine boundary layer". In: *Geophysical Research Letters* 13.2, pp. 125–128.

Janhäll, S., K. F. G. Olofson, P. U. Andersson, J. B. Pettersson, and M. Hallquist (2006). "Evolution of the urban aerosol during winter temperature inversion episodes". In: *Atmospheric Environment* 40.28, pp. 5355–5366.

Jensen, Ø. (2007). "The IMO guidelines for ships operating in Arctic ice-covered waters: From voluntary to mandatory tool for navigation safety and environmental protection". In: *FNI Report* 2.2007, p. 32.

Junninen, H., A. Lauri, P. Keronen, P. Aalto, V. Hiltunen, P. Hari, and M. Kulmala (2009). "Smart-SMEAR: on-line data exploration and visualization tool for SMEAR stations". In: *Boreal Environment Research* 14, pp. 447–457.

Kampa, M. and E. Castanas (2008). "Human health effects of air pollution". In: *Environmental pollution* 151.2, pp. 362–367.

Keller, M. D. (1989). "Dimethyl sulfide production and marine phytoplankton: the importance of species composition and cell size". In: *Biological oceanography* 6.5-6, pp. 375–382.

Kerminen, V.-M., X. Chen, V. Vakkari, T. Petäjä, M. Kulmala, and F. Bianchi (2018). "Atmospheric new particle formation and growth: review of field observations". In: *Environmental Research Letters* 13.10.

Kerminen, V.-M., H. Lihavainen, M. Komppula, Y. Viisanen, and M. Kulmala (2005). "Direct observational evidence linking atmospheric aerosol formation and cloud droplet activation". In: *Geophysical research letters* 32.14.

Khalil, M. and R. Rasmussen (1990). "The global cycle of carbon monoxide: Trends and mass balance". In: *Chemosphere* 20.1-2, pp. 227–242.

King, M. D. and W. R. Simpson (2001). "Extinction of UV radiation in Arctic snow at Alert, Canada (82 N)". In: *Journal of Geophysical Research: Atmospheres* 106.D12, pp. 12499–12507.

Kourtchev, I., C. Giorio, A. Manninen, E. Wilson, B. Mahon, J. Aalto, M. Kajos, D. Venables, T. Ruuskanen, J. Levula, et al. (2016). "Enhanced volatile organic compounds emissions and organic aerosol mass increase the oligomer content of atmospheric aerosols". In: *Scientific reports* 6, p. 35038.

Kulmala, M., H. Vehkamäki, T. Petäjä, M. Dal Maso, A. Lauri, V.-M. Kerminen, W. Birmili, and P. McMurry (2004). "Formation and growth rates of ultrafine atmospheric particles: a review of observations". In: *Journal of Aerosol Science* 35.2, pp. 143–176.

Kulmala, M., M. D. Maso, J. Mäkelä, L. Pirjola, M. Väkevä, P. Aalto, P. Miikkulainen, K. Hämeri, and C. O'dowd (2001). "On the formation, growth and composition of nucleation mode particles". In: *Tellus B* 53.4, pp. 479–490.

Kyrö, E.-M., R. Väänänen, V.-M. Kerminen, A. Virkkula, T. Petäjä, A. Asmi, M. Dal Maso, T. Nieminen, S. Juhola, A. Shcherbinin, et al. (2014). "Trends in new particle formation in eastern Lapland, Finland: effect of decreasing sulfur emissions from Kola Peninsula". In: *Atmospheric Chemistry and Physics* 14.9, pp. 4383–4396.

Laaksonen, A., M. Kulmala, C. O'Dowd, J. Joutsensaari, P. Vaattovaara, S. Mikkonen, K. Lehtinen, L. Sogacheva, M. D. Maso, P. Aalto, et al. (2008). "The role of VOC oxidation products in continental new particle formation". In: *Atmospheric Chemistry and Physics* 8.10, pp. 2657–2665.

Li, S.-M., L. Barrie, R. Talbot, R. Harriss, C. Davidson, and J.-L. Jaffrezo (1993). "Seasonal and geographic variations of methanesulfonic acid in the Arctic troposphere". In: *Atmospheric Environment. Part A. General Topics* 27.17-18, pp. 3011–3024.

Lihavainen, H., V.-M. Kerminen, M. Komppula, J. Hatakka, V. Aaltonen, M. Kulmala, and Y. Viisanen (2003). "Production of "potential" cloud condensation nuclei associated with atmospheric new-particle formation in northern Finland". In: *Journal of Geophysical Research: Atmospheres* 108.D24.

Liu, F., S. Beirle, Q. Zhang, S. Dörner, K. He, and T. Wagner (2016). "NOx lifetimes and emissions of cities and power plants in polluted background estimated by satellite observations". In: *Atmospheric Chemistry and Physics* 16.8, pp. 5283–5298.

Lohmann, U. and J. Feichter (2005). "Global indirect aerosol effects: a review". In: *Atmospheric Chemistry and Physics* 5.3, pp. 715–737.

Lozano, R., M. Hernández-Ceballos, J. Adame, M. Casas-Ruíz, M. Sorribas, E. San Miguel, and J. Bolívar (2011). "Radioactive impact of Fukushima accident on the Iberian Peninsula: evolution and plume previous pathway". In: *Environment international* 37.7, pp. 1259–1264.

Maslanik, J. and J. Stroeve (1999). "Near-real-time DMSP SSM/I-SSMIS daily polar gridded sea ice concentrations". In: *National Snow and Ice Data Center, Boulder, CO, digital media*.

Mauritsen, T., J. Sedlar, M. Tjernström, C. Leck, M. Martin, M. Shupe, S. Sjogren, B. Sierau, P. Persson, I. Brooks, et al. (2011). "An Arctic CCN-limited cloud-aerosol regime". In: *Atmospheric Chemistry and Physics* 11.1, pp. 165–173.

Monks, P. S., A. Archibald, A. Colette, O. Cooper, M. Coyle, R. Derwent, D. Fowler, C. Granier, K. S. Law, G. Mills, et al. (2015). "Tropospheric ozone and its precursors from the urban to the global scale from air quality to short-lived climate forcer". In: *Atmospheric Chemistry and Physics* 15.15, pp. 8889–8973.

Moraes Frasson, R. P. de, L. K. da Cunha, and W. F. Krajewski (2011). "Assessment of the Thies optical disdrometer performance". In: *Atmospheric Research* 101.1-2, pp. 237–255.

Nilsson, E. D. (1996). "Planetary boundary layer structure and air mass transport during the International Arctic Ocean Expedition 1991". In: *Tellus B* 48.2, pp. 178–196.

Nilsson, E., J. Paatero, and M. Boy (2001). "Effects of air masses and synoptic weather on aerosol formation in the continental boundary layer". In: *Tellus B* 53.4, pp. 462–478.

Oltmans, S. J. (1981). "Surface ozone measurements in clean air". In: *Journal of Geophysical Research: Oceans* 86.C2, pp. 1174–1180.

Ounis, H., G. Ahmadi, and J. B. McLaughlin (1991). "Brownian diffusion of submicrometer particles in the viscous sublayer". In: *Journal of Colloid and Interface Science* 143.1, pp. 266–277.

Park, K.-T., S. Jang, K. Lee, Y. J. Yoon, M.-S. Kim, K. Park, H.-J. Cho, J.-H. Kang, R. Udisti, B.-Y. Lee, et al. (2017). "Observational evidence for the formation of DMS-derived aerosols during Arctic phytoplankton blooms". In: *Atmospheric Chemistry and Physics* 17.15, pp. 9665–9675.

Parrish, D., M. Trainer, J. Holloway, J. Yee, M. Warshawsky, F. Fehsenfeld, G. Forbes, and J. Moody (1998). "Relationships between ozone and carbon monoxide at surface sites in the North Atlantic region". In: *Journal of Geophysical Research: Atmospheres* 103.D11, pp. 13357–13376.

Peters, A., H. E. Wichmann, T. Tuch, J. Heinrich, and J. Heyder (1997). "Respiratory effects are associated with the number of ultrafine particles." In: *American journal of respiratory and critical care medicine* 155.4, pp. 1376–1383.

Pruppacher, H. R. and J. D. Klett (2012). *Microphysics of Clouds and Precipitation: Reprinted 1980*. Springer Science & Business Media.

Schutz, L. (1979). "Sahara dust transport over the North Atlantic Ocean-Model calculations and measurements". In: *Saharan Dust: Mobilization, Transport, Deposition*, pp. 267–278.

Sogacheva, L., M. Dal Maso, V.-M. Kerminen, and M. Kulmala (2005). "Probability of nucleation events and aerosol particle concentration in different air mass types arriving at Hyytiälä, southern Finland, based on back trajectories analysis." In: *Boreal Environment Research* 10.6.

Stein, A., R. R. Draxler, G. D. Rolph, B. J. Stunder, M. Cohen, and F. Ngan (2015). "NOAA's HYSPLIT atmospheric transport and dispersion modeling system". In: *Bulletin of the American Meteorological Society* 96.12, pp. 2059–2077.

Stohl, A. (1998). "Computation, accuracy and applications of trajectories - a review and bibliography". In: *Atmospheric Environment* 32.6, pp. 947–966.

Ström, J., J. Umegård, K. Tørseth, P. Tunved, H.-C. Hansson, K. Holmén, V. Wismann, A. Herber, and G. König-Langlo (2003). "One year of particle size distribution and aerosol chemical composition measurements at the Zeppelin Station, Svalbard, March 2000–March 2001". In: *Physics and Chemistry of the Earth, Parts A/B/C* 28.28-32, pp. 1181–1190.

Stull, R. B. (1988). *An Introduction to Boundary Layer Meteorology*. 1st ed. Vol. 13. Springer Netherlands. 670 s.

Stunder, B. J., J. L. Heffter, and R. R. Draxler (2007). "Airborne volcanic ash forecast area reliability". In: *Weather and Forecasting* 22.5, pp. 1132–1139.

Su, L., Z. Yuan, J. C. Fung, and A. K. Lau (2015). "A comparison of HYSPLIT backward trajectories generated from two GDAS datasets". In: *Science of the Total Environment* 506, pp. 527–537.

Tapiador, F. J., F. J. Turk, W. Petersen, A. Y. Hou, E. García-Ortega, L. A. Machado, C. F. Angelis, P. Salio, C. Kidd, G. J. Huffman, et al. (2012). "Global precipitation measurement: Methods, datasets and applications". In: *Atmospheric Research* 104, pp. 70–97.

Thompson, D. W. and J. M. Wallace (1998). "The Arctic Oscillation signature in the wintertime geopotential height and temperature fields". In: *Geophysical research letters* 25.9, pp. 1297–1300.

Tissari, J., J. Lyyränen, K. Hytönen, O. Sippula, U. Tapper, A. Frey, K. Saarnio, A. Pennanen, R. Hillamo, R. Salonen, et al. (2008). "Fine particle and gaseous emissions from normal and smouldering wood combustion in a conventional masonry heater". In: *Atmospheric Environment* 42.34, pp. 7862–7873.

Trigo, R. M., T. J. Osborn, and J. M. Corte-Real (2002). "The North Atlantic Oscillation influence on Europe: climate impacts and associated physical mechanisms". In: *Climate research* 20.1, pp. 9–17.

Väänänen, R., E.-M. Kyrö, T. Nieminen, N. Kivekäs, H. Junninen, A. Virkkula, M. Dal Maso, H. Lihavainen, Y. Viisanen, B. Svenningsson, et al. (2013). "Analysis of particle size distribution changes between three measurement sites in northern Scandinavia". In: *AIP Conference Proceedings*. Vol. 1527. 1, pp. 531–534.

Vanhanen, J., J. Mikkilä, K. Lehtipalo, M. Sipilä, H. Manninen, E. Siivola, T. Petäjä, and M. Kulmala (2011). "Particle size magnifier for nano-CN detection". In: *Aerosol Science and Technology* 45.4, pp. 533–542.

Vehkamäki, H., M. D. Maso, T. Hussein, R. Flanagan, A. Hyvärinen, J. Lauros, P. Merikanto, M. Mönkkönen, K. Pihlatie, K. Salminen, et al. (2004). "Atmospheric particle formation events at Värriö measurement station in Finnish Lapland 1998-2002". In: *Atmospheric Chemistry and Physics* 4.7, pp. 2015–2023.

Vingarzan, R. (2004). "A review of surface ozone background levels and trends". In: *Atmospheric Environment* 38.21, pp. 3431–3442.

Vuoristo, K.-V. (2002). "Regional and structural patterns of tourism in Finland". In: *Fennia-International Journal of Geography* 180.1-2, pp. 251–259.

Weinstock, B. (1969). "Carbon monoxide: Residence time in the atmosphere". In: *Science* 166.3902, pp. 224–225.

Yang, M., T. G. Bell, F. E. Hopkins, and T. J. Smyth (2016). "Attribution of atmospheric sulfur dioxide over the English Channel to dimethyl sulfide and changing ship emissions". In: *Atmospheric Chemistry and Physics* 16.8, pp. 4771–4783.

Yao, L., O. Garmash, F. Bianchi, J. Zheng, C. Yan, J. Kontkanen, H. Junninen, S. B. Mazon, M. Ehn, P. Paasonen, et al. (2018). "Atmospheric new particle formation from sulfuric acid and amines in a Chinese megacity". In: *Science* 361.6399, pp. 278–281.

A. Timeseries of SMEAR I Observations

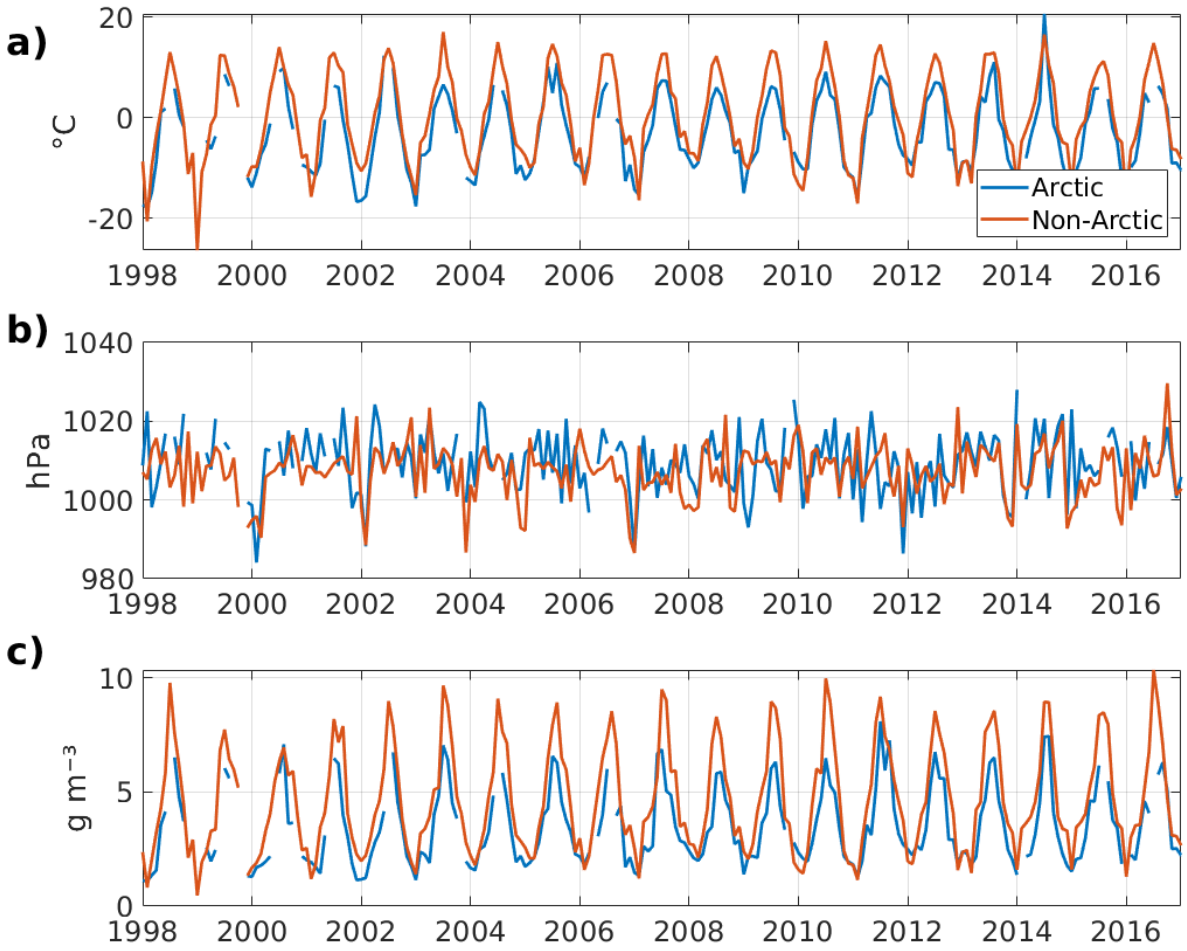

Figure A.1: Monthly median values of a) temperature, b) air pressure (reduced to sea level) and c) absolute humidity in 1998-2017 for Arctic (blue) and non-Arctic (red) air masses. The data are from SMEAR I, Värriö.

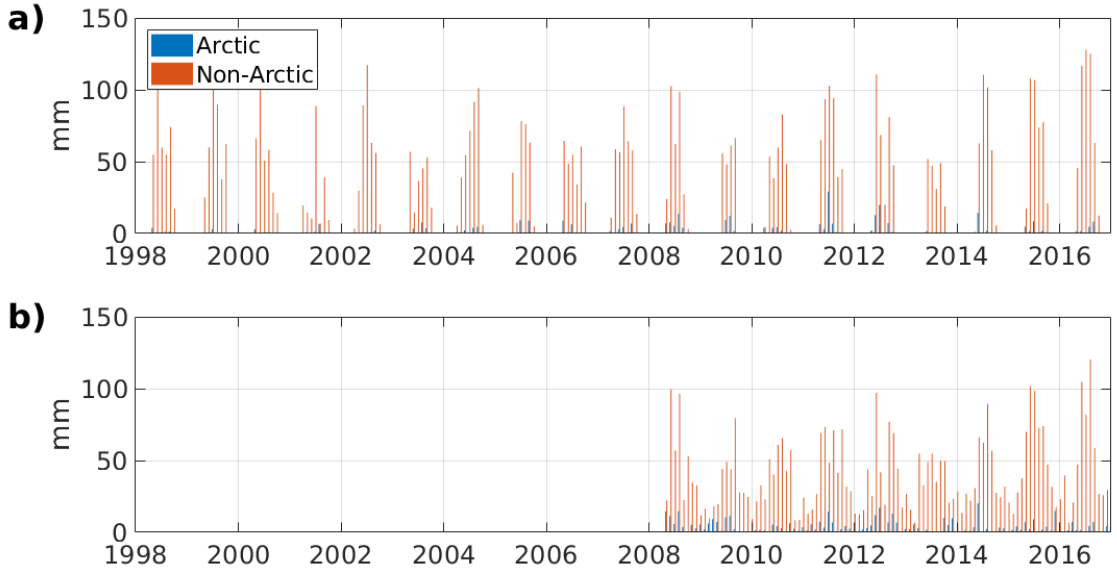

Figure A.2: Monthly sum of precipitation using two instruments: a) tipping-bucket type rain gauge and b) laser disdrometer in 1998-2017 for Arctic (blue) and non-Arctic (red) air masses. The data are from SMEAR I, Värriö. The laser disdrometer was installed in 2008.

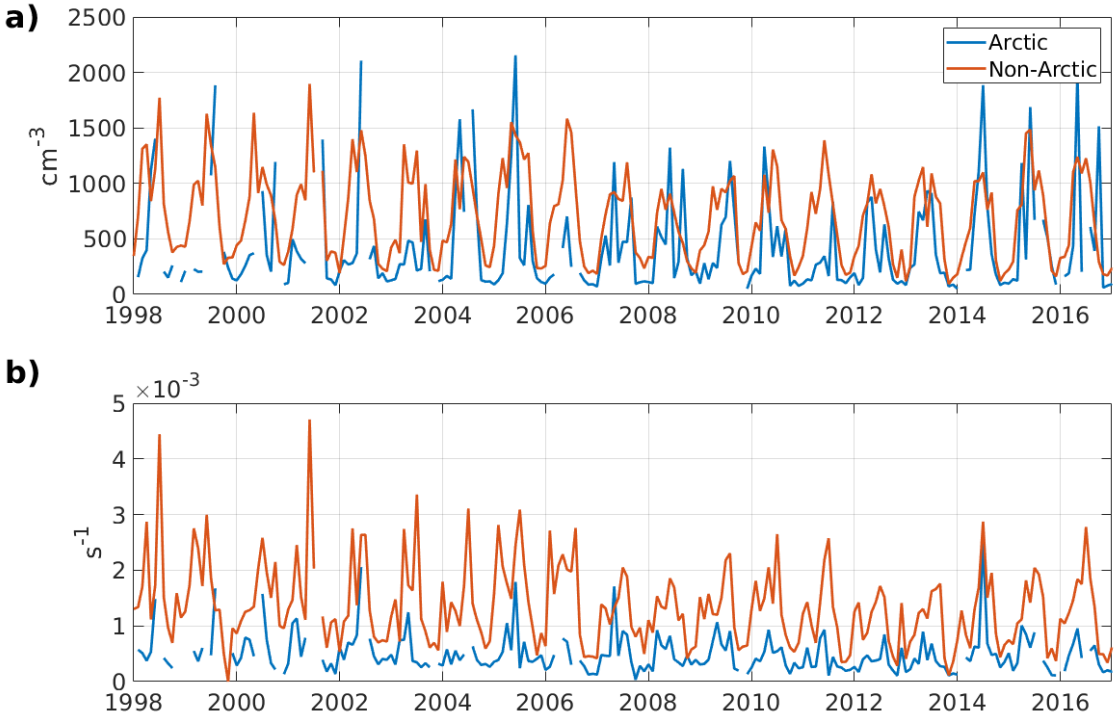

Figure A.3: Monthly median values of a) total particle concentration and b) condensation sink (CS) in 1998-2017 for Arctic (blue) and non-Arctic (red) air masses. The data are from SMEAR I, Värriö.

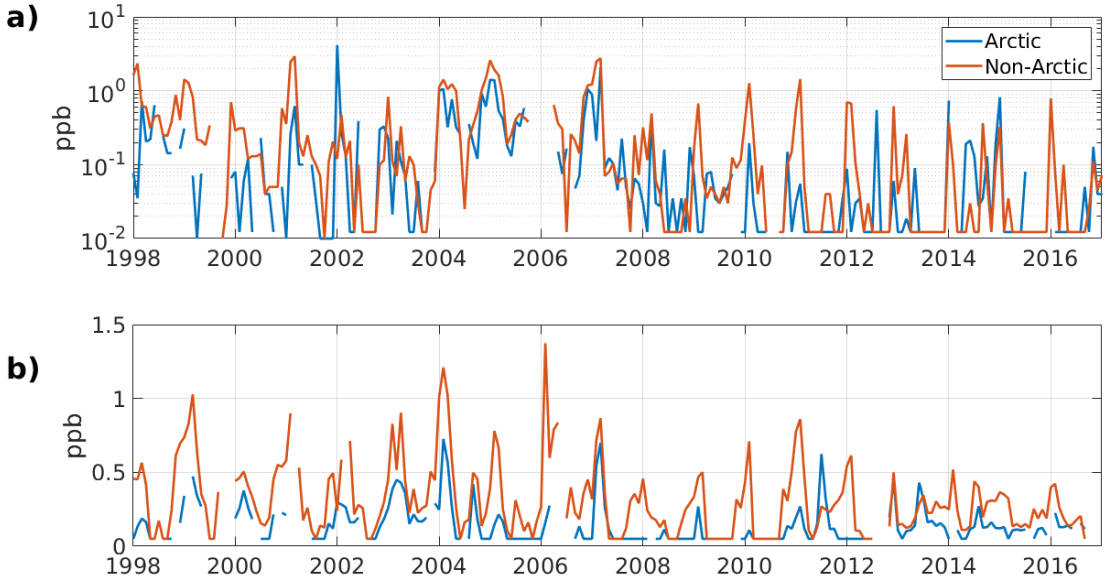

Figure A.4: Monthly median values of a) sulphur dioxide (SO_2) and b) nitrogen oxides (NO_X) in 1998-2017 for Arctic (blue) and non-Arctic (red) air masses. The data are from SMEAR I, Värriö.

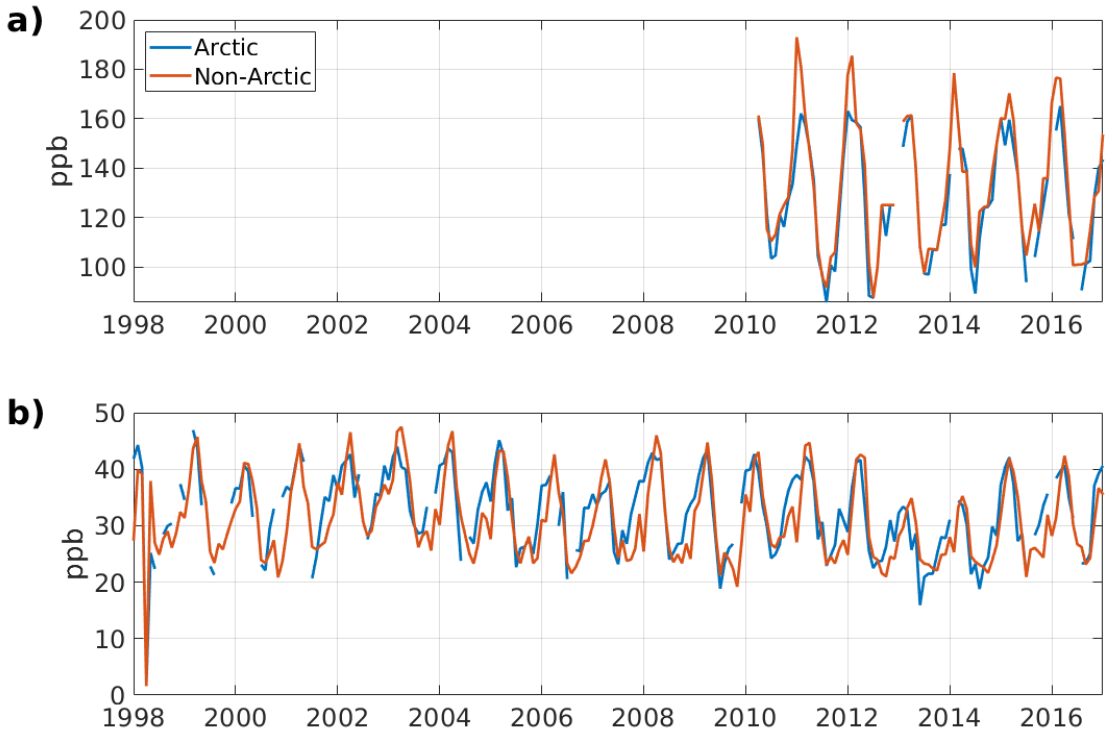

Figure A.5: Monthly median values of a) carbon monoxide (CO) and b) ozone (O_3) in 1998-2017 for Arctic (blue) and non-Arctic (red) air masses. The data are from SMEAR I, Värriö. The measurements of CO began in 2010.